Eur. Phys. J. B (2018) 91: 142
https://doi.org/10.1140/epjb/e2018-90114-9

THE EUROPEAN PHYSICAL JOURNAL B

Regular Article

Linear response time-dependent density functional theory of the Hubbard dimer*

Diego J. Carrascal[1,2], Jaime Ferrer[1,2,a], Neepa Maitra[3], and Kieron Burke[4]

[1] Department of Physics, Universidad de Oviedo, 33007 Oviedo, Spain
[2] Nanomaterials and Nanotechnology Research Center, CSIC/Universidad de Oviedo, Oviedo, Spain
[3] Department of Physics, Hunter College, City University of New York, New York, NY 1006, USA
[4] Department of Chemistry and of Physics, University of California, Irvine, CA 92697, USA

Received 1 March 2018 / Received in final form 3 May 2018
Published online 2 July 2018

Abstract. The asymmetric Hubbard dimer is used to study the density-dependence of the exact frequency-dependent kernel of linear-response time-dependent density functional theory. The exact form of the kernel is given, and the limitations of the adiabatic approximation utilizing the exact ground-state functional are shown. The oscillator strength sum rule is proven for lattice Hamiltonians, and relative oscillator strengths are defined appropriately. The method of Casida for extracting oscillator strengths from a frequency-dependent kernel is demonstrated to yield the exact result with this kernel. An unambiguous way of labelling the nature of excitations is given. The fluctuation-dissipation theorem is proven for the ground-state exchange-correlation energy. The distinction between weak and strong correlation is shown to depend on the ratio of interaction to asymmetry. A simple interpolation between carefully defined weak-correlation and strong-correlation regimes yields a density-functional approximation for the kernel that gives accurate transition frequencies for both the single and double excitations, including charge-transfer excitations. Many exact results, limits, and expansions about those limits are given in the Appendices.

1 Introduction

Time-dependent density functional theory (TDDFT) is a popular first-principles approach to calculating low-lying optical excitations of molecules [1–3]. A typical calculation first involves optimizing the structure within ground-state DFT using some approximate exchange-correlation functional. Then a linear-response TDDFT calculation, usually solving RPA-type equations in frequency space [4–7], or via real-time propagation [8], yields both transition frequencies and oscillator strengths. The TDDFT step almost always makes the adiabatic approximation for the unknown and (generally) frequency-dependent exchange-correlation (XC) kernel, in which its zero-frequency limit is used [9]. This is simply the second functional-derivative of the exchange-correlation energy of ground-state DFT. Usually, the same approximate XC functional is used for the first ground-state step and for the TDDFT step. Several thousand papers per year use this method to extract useful information on electronic excitations, with typical transition frequency errors of order 0.25–0.5 eV [10–14].

However, in the three decades since the Runge-Gross theorem established the formal exactitude of this approach [1], a variety of situations have been identified where approximations fail, often qualitatively. Among the most notorious are failures for charge-transfer excitations, whose transition frequencies are typically grossly underestimated by the standard functionals [15–20], but reasonable results can be obtained by using range-separated hybrids [21–25]. Another one is the complete absence of double-excitations from the spectrum within the adiabatic approximation [26–28]. Initial hopes of extracting double-excitations from higher-order response theory were dashed by reference [29,30]. A simple model of the frequency dependence for the specific case of a double excitation close to one or a few single excitations in a weakly correlated system [28,31], is a useful tool for a post-adiabatic TDDFT treatment called dressed TDDFT, and has been applied to a range of systems [32–34] but has not been widely adopted.

While practical electronic structure calculations begin from the real-space Hamiltonian, much useful insight and even semi-quantitative results can be extracted from model Hamiltonians, especially when correlations are strong [35,36]. The paradigmatic case in condensed matter is the (one-band) Hubbard model, which is usually taken on an infinite lattice, and can be analyzed in 1-, 2-, or 3 dimensions. The model is characterized by only two

* Contribution to the Topical Issue "Special issue in honor of Hardy Gross", edited by C.A. Ullrich, F.M.S. Nogueira, A. Rubio, and M.A.L. Marques.

[a] e-mail: ferrer@uniovi.es

parameters, a hopping energy between nearest neighbours t and an on-site Coulomb repulsion for doubly-occupied sites U, and site-occupation plays the role of the density. Model Hamiltonians are not aimed at high levels of quantitative accuracy, but are designed to explore qualitative features of correlation physics. For example, the 2D Hubbard model may display the essential features of high-temperature superconductivity [37–39].

Thus, Hubbard (and more complex) chains have been used to study, e.g., correlation effects in transport through single molecules and small quantum dots. They have also been used to explore full time propagation in TDDFT, going beyond the linear response regime [40–56]. It is usually relatively straightforward to exactly solve the time-dependent Schrödinger equation in these cases. It can also be easy to find the exact ground-state density functional [47,50,57–59], and to propagate the fully time-dependent Kohn-Sham equations within the adiabatically exact approximation, in order to study its capabilities and limitations.

Interestingly, among all the papers using TDDFT in lattice models, relatively few have studied frequency-domain linear-response TDDFT (lrTDDFT) in interacting systems [49,56,60]. In the case of the two-site Hubbard dimer, Aryasetiawan and Gunnarson [60] did groundbreaking work in studying the performance of lrTDDFT for the symmetric dimer. However, as emphasized in a recent review focussed solely on ground-state DFT for the dimer [61], many crucial DFT features can only be seen when the dimer is made asymmetric via a difference in the on-site potentials Δv [47,57]. In fact one cannot really speak of density-functionals if restricting to symmetric cases, since there is no dependence on the ground-state density, as the site occupations always remain identical. In addition, the Kubo response of the asymmetric dimer shows two excitations, while only one survives in the symmetric case. Again, a few recent works have noted this effect [47].

In the present article, we thoroughly explore the asymmetric dimer within lrTDDFT, finding the exact non-adiabatic density-functional for the exchange-correlation kernel. In previous works [62,63] the exact frequency-dependent kernel has been found for a given system: in reference [63] an analytic expression is derived for a homogeneous two-electron density on a ring while in reference [62] a general numerical procedure is given for computing the kernel of a given system. This is, we believe, the first time that the exact frequency-dependent kernel as a functional of the ground-state density has been found for any model; the Hubbard model is simple enough to allow for a complete analytic study. We find that correlations are suppressed by asymmetry, so that a weak correlation approximation remains accurate even when the ratio between the Coulomb repulsion U and the hopping integral t is very large, as long as the asymmetry between the on-site energies Δv is also large. In fact, for sufficiently large $\Delta v/U$, this weakly correlated kernel remains accurate, no matter how large U/t is. Only when U is large relative to both $2t$ and Δv does the weak-correlation kernel fail. Moreover, a simple expansion about the strongly-correlated limit, which we call the Mott-Hubbard (MH) regime, suffices for all other cases, so that an appropriate interpolation between the two yields accurate results for almost all parameter values. Thus we have found an accurate approximate kernel for both double and charge-transfer excitations, that works in both weak and strong correlation regimes. We note that this provides a useful explicit example of the frequency-dependence of the kernel as a functional of the ground-state density for this model, but does not produce a general purpose density functional for this frequency dependence.

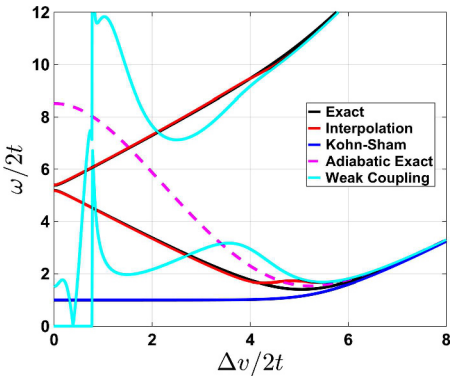

Fig. 1. Transition frequencies ω as a function of onsite potential asymmetry, Δv for $U = 10\,t$. Black lines are exact, blue are the transitions of the KS electrons with the exact ground-state functional, dashed magenta includes TDDFT corrections with an adiabatically exact kernel, i.e., using the exact ground-state functional in TDDFT. The cyan line shows TDDFT with a weak-correlation approximation to the kernel, which diverges for sufficiently small asymmetry. The red line is the interpolation kernel developed in this work. Within this figure, the exact and interpolation lines can hardly be distinguished.

To illustrate these results we plot in Figure 1 the transition frequencies for both singlet excitations when the dimer is strongly-interacting ($U = 10\,t$) as a function of asymmetry, Δv. In the symmetric limit ($\Delta v = 0$), the two excited states are barely separated. Because correlation is strong, the KS transitions are a poor approximation to the exact ones, and even the adiabatically-exact correction to TDDFT does not really improve matters. It vastly overestimates the correction to the single excitation and, being adiabatic, yields no prediction for the double excitation at all. The interpolation kernel developed here, which interpolates between the weakly and strongly correlated limits, is almost perfect for these transition frequencies. Note how, if the asymmetry is comparable to U or larger, then the weak-coupling approximation works well. We explain this feature in this work.

While this article may appear long, its main results can be easily summarized. In Section 3, we give a very detailed account of how lrTDDFT behaves exactly for the Hubbard dimer. This is a beautifully simple case, with a very limited Hilbert space, in which the (usually unknown) XC kernel of TDDFT can be written exactly and explicitly (at least as function of the potential), including the frequency-dependence needed to generate the double excitation. This can be thought of as a many-body person's guide to

TDDFT. On the other hand, in Section 4, we explore meatier issues of approximations. We begin with weakly correlated systems (Sects. 4.2 and 4.3) and show how the usual approximations work in the usual way for such systems, drawing the analogy with dressed TDDFT, which is a specific approximation to the frequency-dependent kernel that captures double excitations in this regime. But we also explore the strongly-correlated (Mott-Hubbard) limit (Sects. 4.4 and 4.5), and show how to distinguish weak and strong correlation in this case. We perform the necessary expansions in the two limits (Appendix C), and construct an interpolation scheme for the kernel that gives highly accurate results in both regimes, and reasonably accurate results in the interpolative regime (Sect. 4.6).

For those with an interest and background in TDDFT, some key results to take away include a general discussion of state labelling (how do you classify something as a double excitation?: see Sects. 3.1 and 3.2), defining (relative) oscillator strengths in lattice models (see the same section and Sect. 3.2), confirmation that the oscillator strength of a double can be extracted from Casida's matrix formulation (Sect. 3.4), and illustration that a pole in the kernel produces a double excitation, as in dressed TDDFT. For those with a background in many-body theory, some other key results are the separation of Mott-Hubbard and weakly correlated regimes (Sect. 4.4 and Fig. 7), and generalizations to site-dependent U (Appendix B.3) and fractional particle numbers (Appendix B.4). The exact formulas (Appendix A.1) and expansions and limits (Appendix C) should prove very useful to anyone using Hubbard Hamiltonians with any background.

Finally, we include here a table of notation that should help any reader dealing with the many symbols used here (Tab. 1).

Table 1. Our Hubbard dimer notation. The dimensionless variables are set in units of twice the hopping unless otherwise stated. A subscript s denotes a Kohn-Sham counterpart of any variable.

Definition	Description
t	Hopping
U	Coulomb interaction, Hubbard U
v_1, $v_2 = -v_1$	On-site potentials
$\Delta v = v_2 - v_1$	On-site potential difference
n_1, n_2	Site occupations
N or $\mathcal{N}$	Electron number
$\Delta n = n_1 - n_2$	Occupation difference
$\rho = \lvert\Delta n\rvert/2$	Useful alternative to Δn
$\lvert\Psi_i\rangle$, E_i, ω_i	Exact states, energies, and transitions
W_i	Exact excitation weights
f	relative oscillator strength of 2nd excitation
MHn	Mott-Hubbard expansion to nth order
WCn	Small-U expansion to nth order
Dimensionless variables	
$u = U/2t$	Dimensionless Hubbard U
$x = \Delta v/2t$	Dimensionless potential difference
$z = x/u$	Potential difference in units of U
$\bar{u}, \bar{x}, \bar{z}$	Reduced variables, ranging from 0 to 1
$x_s = \Delta v_s/2t$	Kohn-Sham potential difference
$e_i = E_i/2t$, ν_i	Dimensionless energies and frequencies
ν_3, ν_4	Auxiliary frequencies
χ	dimensionless response function
$\chi_{\rm AE}$	Adiabatic approximation to χ
a, b, c, ν_f	Exact response function parameters
$f_{\rm HXC}$	Hartree-exchange-correlation kernel
$f_{\rm st}$, $f_{c,\rm dyn}$	Stationary and dynamic part of the kernel

2 Background

2.1 Time-dependent DFT

Time-dependent density functional theory (TDDFT) is based on the Runge-Gross theorem [1], which is derived in a very different way from the Hohenberg-Kohn theorem of ground-state DFT [64]. The theorem proves a one-to-one correspondence between time-dependent densities and one-body potentials, for a given initial-state, particle-particle interaction, and statistics. Applied to electrons starting in a non-degenerate ground-state, and using the Hohenberg-Kohn result that the ground-state wavefunction is a functional of the ground-state density, it implies that all properties of the many-body system can be extracted from knowledge of its time-dependent density alone.

TDDFT can be and is applied to many-electron systems driven by arbitrarily strong laser fields [3,9], but the vast majority of applications use results from linear-response. Defining the density-density response function of a system as

$$\chi(\mathbf{r},\mathbf{r}',t-t') = \left.\frac{\delta n(\mathbf{r},t)}{\delta v_{\rm ext}(\mathbf{r}',t')}\right|_{n=n_0(\mathbf{r})}, \qquad (1)$$

where $n_0(\mathbf{r})$ is the ground-state density, analysis leads to the famous Dyson-like equation [65]:

$$\chi(\omega) = \chi_{\rm S}(\omega) + \chi_{\rm S}(\omega) \star (f_{\rm H} + f_{\rm XC}(\omega)) \star \chi(\omega), \qquad (2)$$

where $\star$ denotes matrix multiplication in $\mathbf{r}$-space (given two real-space functions, $f(\mathbf{r},\mathbf{r}')$ and $g(\mathbf{r},\mathbf{r}')$, matrix multiplication means $\int d\mathbf{r}''\, f(\mathbf{r},\mathbf{r}'')\, g(\mathbf{r}'',\mathbf{r}'))$. $\chi(\omega) = \chi(\mathbf{r},\mathbf{r}',\omega)$ is the Fourier transform of $\chi(\mathbf{r},\mathbf{r}',t-t')$, $\chi_{\rm S}(\omega)$ is its non-interacting KS analog, while $f_{\rm H} = 1/|\mathbf{r}-\mathbf{r}'|$ is the Hartree kernel and $f_{\rm XC}(\omega) = f_{\rm XC}[n_0](\mathbf{r},\mathbf{r}',\omega)$ is the frequency-dependent XC kernel, a functional of the ground-state density. The latter is the time-Fourier transform of $\delta v_{\rm XC}(\mathbf{r},t)/\delta n(\mathbf{r}',t')$. This Dyson-like RPA-like equation can in principle be solved for the exact χ, which has poles at all optically-allowed excitations of the system.

For molecules, equation (2) is often re-cast in the form of a matrix equation in the space of single KS excitations. These can be derived and represented in several ways [4,6,7,66], but all are essentially equivalent to finding eigenvalues and eigenvectors of the matrix

$$R_{qq'}(\omega) = \omega_q^2\,\delta_{qq'} + 4\sqrt{\omega_q\omega_{q'}}\, f^{qq'}_{\rm HXC}(\omega)\,, \qquad (3)$$

where

$$f^{qq'}_{\rm HXC}(\omega) = [q|f_{\rm H} + f_{\rm XC}(\omega))|q'], \qquad (4)$$

and $q = (i, a)$ represents a double-index, with i labelling an occupied orbital and a an unoccupied one, with

$$[\,q|f_{\rm XC}(\omega)|q'\,] = \int d^3r\, d^3r'\, \Phi_q(\mathbf{r})\, f_{\rm XC}(\mathbf{r},\mathbf{r}',\omega)\, \Phi_{q'}(\mathbf{r}'), \quad (5)$$

and $\Phi_q = \phi_i^* \phi_a$. The eigenvalues of the matrix equation (3) are the squares of the transition frequencies ω_I, and oscillator strengths out of the ground-state, f_I, can be extracted from the eigenvectors. The latter satisfy the Thomas-Reiche-Kuhn (TRK) sum rule [67–69]

$$\sum_I f_I = N. \quad (6)$$

In principle, both the transition frequencies and oscillator strengths are given exactly when both exact ground-state and time-dependent DFT are used. Even with the exact ground-state functional, the KS response function has poles only at single excitations and, in the adiabatic approximation, the excitations resulting from solving the matrix equations yield only linear combinations of single excitations. The frequency-dependence of $f_{\rm XC}$ generates the states of multiple-excitation character.

Practical DFT calculations require functional approximations. In most applications of TDDFT, the adiabatic approximation is made, allowing both the kernel and the starting point to be approximated via ground-state functionals. Such an approximation is usefully accurate for many low-lying excitations of chemical interest [10–14]. However, much experience has been gained on where standard semilocal approximations, applied in this way, fail quantitatively or even qualitatively, including Rydberg excitations, charge-transfer excitations, double excitations, conical intersections, the thermodynamic limit, etc. [9] More sophisticated functionals have been shown to offer a good solution to several of these cases. Many of these failures can be traced to errors made in the ground-state part of the calculation; these can be eliminated by using the exact ground-state functional, when available, for simple model systems.

Some years ago, a modest proposal was made for recovering double excitations in lrTDDFT, at least in cases where the double was close to one or more single excitations, and correlations were weak [28,31]. By reverse engineering the exact wavefunctions in such a case, the frequency-dependent kernel of dressed TDDFT was proposed:

$$2[q|f_{\rm XC}(\omega)|q] = 2[q|f_{\rm XC}^A|q] + \frac{|H_{qD}|^2}{\omega - (H_{DD} - H_{00})}, \quad (7)$$

for the case of a KS single excitation $q = i \to a$ mixing with a KS double excitation D. Here, $f_{\rm XC}^A$ is an adiabatic approximation to the kernel, and H_{IJ} are matrix elements of the full Hamiltonian between the KS states indicated. The additional pole in this kernel generates a double excitation at approximately the correct transition frequency when the system is weakly correlated.

2.2 Asymmetric Hubbard dimer

We analyse here the asymmetric Hubbard dimer model with two opposite-spin fermions:

$$\begin{aligned}\hat{H} &= -t \sum_\sigma (\hat{c}_{1\sigma}^\dagger \hat{c}_{2\sigma} + h.c) + U \sum_i \hat{n}_{i\uparrow}\, \hat{n}_{i\downarrow} + \sum_i v_i \hat{n}_i \\ &= \hat{T} + \hat{V}_{ee} + \hat{V}_{\rm ext}. \end{aligned} \quad (8)$$

We set $\bar{v} = (v_1 + v_2)/2 = 0$ and rewrite the external potential term as $V_{\rm ext} = -\Delta v\, \Delta n/2$, where $\Delta v = v_2 - v_1$ and $\Delta n = n_1 - n_2$. We use $2t$ to set the energy scale, and so define dimensionless measures of the interaction strength $u = U/2\,t$ and the asymmetry $x = \Delta v/2\,t$. The Hamiltonian has three basis states within the sub-space $N = 2$, $S^2 = 0$, $S_z = 0$, so that it can be diagonalized analytically yielding a ground state and two excited states with energies e_i and wave functions Ψ_i, $i = 0, 1, 2$. Explicit expressions are given in Appendix A.1.

The asymmetric dimer makes a beautiful illustration of all the principles of TDDFT, because so many confusing features of TDDFT have explicit formulas in this case due to the very small Hilbert space [58]. A recent review of simply ground-state DFT using the asymmetric dimer references the substantial literature on this [61]. The density functional for fixed integer particle number N is just a function of the site occupation difference Δn, and the KS system is just an asymmetric tight-binding problem. Explicit formulae for fractional particle numbers $\mathcal{N}$ can also be drawn. Many features, from the effect of strong correlation on the Green's function, to the derivative discontinuity correction to the gap at integer N, can be calculated exactly and often explicitly. While the XC energy functional cannot be written analytically, a parametrization given in reference [61] is so accurate as to make no discernible error on the scale used here. It can also be simply generalized to include distinct Coulomb energies on the two sites, and so include the 2-site Anderson model as a special case (see Appendix B.3).

3 Linear response

For the present purpose, we must go beyond just ground-state properties, and calculate the excited state energies and "optical" response. We confine ourselves to spin-conserving perturbations. We emphasize that several results in this section already appear elsewhere, although not in the forms presented here.

We will be interested in extracting information about excitations in response to a weak perturbation. Define the dimensionless density-density linear response function,

$$\tilde{\chi}(t,t') = \begin{pmatrix} \delta\Delta n(t)/\delta x(t')|_{\Delta n_0, N_0} & \delta N(t)/\delta x(t')|_{\Delta n_0, N_0} \\ \delta\Delta n(t)/\delta \bar{v}(t')|_{\Delta n_0, N_0} & \delta N(t)/\delta \bar{v}(t')|_{\Delta n_0, N_0} \end{pmatrix}. \quad (9)$$

However, $\hat{N}$ commutes with the Hamiltonian and we work in this article in a subspace with definite N $(= N_0 = 2)$. As a consequence, only $\chi(t,t) = \delta\Delta n(t)/\delta x(t')|_{\Delta n_0, N_0}$ is

different from zero and we drop henceforth the subindex N_0. Nothing forbids choosing subspaces with non-definite value of N, it is just more complicated [58], and in this case the four matrix elements would be non-zero.

3.1 Many-body theory

We work from now on with $\chi(t,t) = \delta\Delta n(t)/\delta x(t')|_{\Delta n_0, N_0}$; whose Fourier transform with respect to $t-t'$ gives, in the Lehmann representation [70],

$$\chi(\nu) = \frac{2\,\nu_1\,W_1}{\nu_+^2 - \nu_1^2} + \frac{2\,\nu_2\,W_2}{\nu_+^2 - \nu_2^2}, \tag{10}$$

where $\nu_+ = \nu + i\,\delta$, $\nu = \omega/2t$ are dimensionless frequencies and the infinitesimal positive number δ enforces the causality of the response function and shifts the poles infinitesimally below the real axis. (Here χ is $2t$ times the dimensional tight-binding version of Eq. (1).) The two excitations are characterised by their frequencies and weights,

$$\nu_i = e_i - e_0, \quad W_i = |\langle\Psi_0|\Delta\hat{n}|\Psi_i\rangle|^2 \tag{11}$$

whose explicit expressions are given in Appendix A.1. We define as "first" and "second" excitations always ν_1 and ν_2 respectively, e.g., "first" is the lower and "second" is the higher of the two excitations of the Hubbard dimer. The weight of the second excitation vanishes in the symmetric case: much of what can be learned about how TDDFT works for strongly correlated cases requires asymmetry. The frequency integral of the imaginary part of $\nu\chi(\nu)$ is (see Appendix B.1):

$$-\int_0^\infty \frac{d\,\nu}{\pi}\,\mathrm{Im}\,\chi(\nu)\,\nu = \nu_3 = \nu_1\,W_1 + \nu_2\,W_2. \tag{12}$$

For a real-space Hamiltonian, this integral satisfies the TRK sum rule [67–69], where the right hand-side is just N, and so can be used to define oscillator strengths. Because of the lattice nature of the model, this rule is not true here [71–73], and the right-hand side is not a universal value, independent of the interaction or potential. We define a relative oscillator strength for the second excitation as

$$f = \frac{\nu_2\,W_2}{\nu_1\,W_1 + \nu_2\,W_2} = \frac{\nu_2\,W_2}{\nu_3}, \tag{13}$$

so that equation (10) can instead be written as

$$\chi(\nu) = 2\nu_3\left(\frac{1-f}{\nu_+^2 - \nu_1^2} + \frac{f}{\nu_+^2 - \nu_2^2}\right). \tag{14}$$

Throughout our analysis, we will also use an equivalent form, namely

$$\chi^{-1}(\nu) = a\,\nu_+^2 - c - \frac{b\,\nu_+^2}{\nu_+^2 - \nu_f^2}, \tag{15}$$

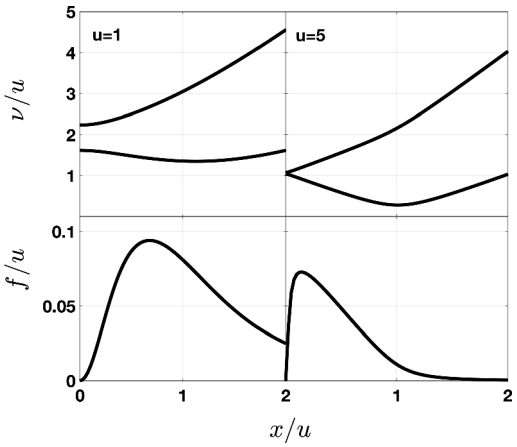

Fig. 2. Transition frequencies of the first and second excitations and oscillator strength of the second excitation as a function of onsite potential asymmetry $x = \Delta v$, for $u = 1$ and $u = 5$, where $2t = 1$.

where, defining

$$\nu_4 = \nu_1\,W_2 + \nu_2\,W_1, \quad \nu_f = \sqrt{\frac{\nu_1\nu_2\nu_4}{\nu_3}}, \quad \bar{\nu}_f = \nu_f\frac{\nu_3}{\nu_4}, \tag{16}$$

then, with $\Delta\nu = \nu_2 - \nu_1$, $\Delta\nu_f = \bar{\nu}_f - \nu_f$:

$$a = \frac{1}{2\nu_3}, \quad \frac{b}{a} = \Delta\nu^2 - \Delta\nu_f^2, \quad c = \frac{\nu_1\,\nu_2}{2\,\nu_4}. \tag{17}$$

Thus the response can be characterized by four functions (a, b, c and ν_f) of the basic reduced variables u and x, which can be deduced from equations (10), (12), and (15). We will consider many approximations to χ, but all will have the same form as the exact χ of equation (15), and therefore can be defined in terms of a, b, c, and ν_f.

Figure 2 shows the transition frequencies and relative oscillator strength f (of the second excitation) as a function of the dimensionless potential asymmetry $x = \Delta v/2t$ for two different values of u. On the left, $u = 1$ and the system is weakly interacting. The first excitation frequency initially drops with x, with the correction being $(1-3u)x^2/2$, but eventually grows as x when x is larger than u. The second excitation has no linear correction in u, and so behaves largely as its non-interacting value, being 2 in the symmetric case, and $2x$ for large x. The situation is very different when interaction is strong ($u = 5$). Now, the frequency of the two excitations equals about u in the symmetric limit. These frequencies split linearly however as x grows as $u \pm x$ all along the Mott-Hubbard (MH) regime, that covers all values of x smaller than u (see Sect. 4.4). This behaviour changes as soon as x becomes larger than u, where the system enters the charge-transfer (CT) regime. Subsequently, the frequency of the first excitation grows like $x - u$, while that of the second grows like $2\,x$. The gap between the two hence grows linearly along the CT regime at a rate of $x + u$. So we find that the excitations behave the same for any value of u, for sufficiently large x. We will see later (Sect. 4.4) that *sufficiently* means

$x > u$, hence the CT regime. They however behave very differently for small and for large u for small values of x, marking the MH regime $u > x$.

It is useful to consider the nature of the ground and excited states in the extreme MH and CT limits to further understand these curves. Simplified expressions for the three states in these limits can be found in Appendix C.5. In the MH limit of very large u/x (i.e., towards the left of each plot in Fig. 2), the ground-state approaches one fermion on each site. This means the lowest excitation transfers one fermion to the lower site, costing an energy of $u - x$, while the second excitation transfers one fermion to the upper site, costing an energy of $u + x$. On the other hand, in the CT limit of u/x very small, the ground-state approaches the situation where both fermions sit on the lower site. The lowest excitation transfers one electron to the other site, costing an energy of $-u + x$, while the second excitation transfers both to the upper site, costing an energy of $2x$ relative to the ground-state. These limiting behaviors are evident in the plots above.

3.2 KS response

In the previous section, we discussed our system within a traditional many-body framework, with all parameters considered as functions of u and $x = \Delta v/2t$, the interaction and one-body potential respectively. This next section is devoted to showing how this system is treated exactly from a TDDFT viewpoint, using the ground-state density in place of the one-body potential. Notice that we are working within the sub-space $N = 2$. However, we write down analytical formulae for the KS response function for fractional occupation numbers $\mathcal{N} \in [0, 4]$ in Appendix B.4. Knowledge of the dependence of the full response function on $\mathcal{N}$ relies on a complete analysis of the dependence of the XC kernel on $\mathcal{N}$, which is beyond the scope of this article. The ground-state DFT analysis of the Hubbard dimer for arbitrary integer or fractional $\mathcal{N}$ groundstate was discussed in detail in reference [61].

The exact ground-state KS system is simply the asymmetric tight-binding model whose ground-state site occupation difference matches that of the interacting system, i.e., $x_{\rm S}(\rho) = \Delta v_s/2t = \rho/r$, where $\rho = |\Delta n|/2$ is the *exact* interacting ground-state density and where $r = \sqrt{1-\rho^2}$. Thus it is trivial to construct the KS potential as a function of the ground-state density. The tight-binding model has two orbitals, the lower being doubly occupied and the higher unoccupied in the ground state. These fictitious KS electrons have a response function

$$\chi_s(\nu) = \frac{2\,\nu_s\,W_s}{\nu_+^2 - \nu_s^2}, \tag{18}$$

where

$$\nu_s = \sqrt{1 + x_s^2} = \frac{1}{r}, \quad W_s = \frac{2}{1 + x_s^2} = 2\,r^2. \tag{19}$$

Thus

$$\chi_s^{-1} = a_s\,\nu_+^2 - c_s, \tag{20}$$

where $a_{\rm S} = 1/4r$ and $c_{\rm S} = 1/4r^3$. Notice that the KS pole corresponding to the second excitation has zero weight, i.e., $f_{\rm S} = 0$, $b_{\rm S} = 0$. This expression for χ_s is generalized to fractional particle number in Appendix B.4.

We end this section with a digression to give a general definition of the nature of an excitation within TDDFT. Our definition applies whenever the exact KS ground-state wavefunction is a single slater determinant, but can easily be generalized beyond that. In such a case, the nature of an excitation of the KS system is clear, e.g., a double excitation is a slater determinant with two electrons excited from their ground-state orbitals. We note that the Hilbert space of states of the system is classified into subspaces labelled unambiguously with every set of quantum numbers available, that includes N. Then, the number of KS slater determinants and the number of exact many-body states in every subspace is the same. As a consequence, each many-body excitation can be continuously connected to a well-labelled KS state via the adiabatic connection, i.e., by following its behavior as a function of λ, while keeping the ground-state density fixed. This gives an unambiguous labelling to each level of the many-body system. This is the natural choice within KS DFT. It differs from that of wavefunction theory, which usually starts from the HF wavefunction. The differences are small for weakly correlated systems, but can be quite large when correlation is strong. In fact, when an unrestricted HF calculation breaks symmetry, this creates difficulties in using the HF wavefunction as a reference. Here, the exact ground-state KS wavefunction is always a doubly occupied singlet, and so does not suffer from this difficulty.

We follow this procedure here, and show, in strongly correlated cases that, even when the interacting wavefunction is a mixture of several determinants, its label remains unambiguous. Of course, when correlations are strong, the overlap between the many-body and KS wavefunctions is often much less than 1, but this is also true in the ground-state theory. This definition must be applied carefully when curves cross or in the thermodynamic limit, where there are infinitely many states. In Appendix C.5, we show how the many-body and KS states behave in the dissociation limit. The adiabatic connection between the many-body and KS wavefunctions can be traced down analytically in this limit, keeping the density fixed, and so determine the nature of the wavefunctions, even though their overlap at full-coupling is much less than 1.

3.3 Exchange-correlation kernel

From equation (2), the Hartree-exchange-correlation kernel is defined by the difference of the true inverse response function from the KS inverse response function

$$f_{\rm HXC}(\nu) = \chi_{\rm S}^{-1}(\nu) - \chi^{-1}(\nu). \tag{21}$$

This is in general a frequency-dependent quantity, but in almost all TDDFT calculations, it is approximated by its static limit $f_{\rm st} = f_{\rm HXC}(0)$. For any finite system, this is exactly given by ground-state DFT, and here

$$f_{\rm st} = c - c_{\rm S}. \tag{22}$$

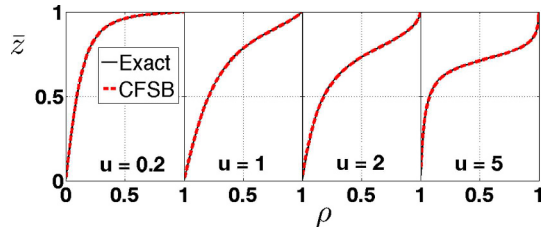

Fig. 3. Exact (black) and CFSB (dashed red) reduced external potential $\bar{z} = z/\sqrt{1+z^2}$, where $z = x/u$, as a function of $\rho = |\Delta n|/2$ for $u = 0.2$, 1, 2 and 5 ($2t = 1$).

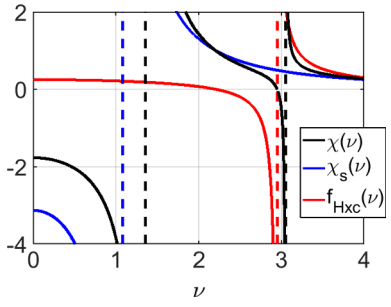

Fig. 4. Frequency dependence of exact (black) and Kohn-Sham susceptibilities (blue) and exchange-correlation kernel (red line) for $u = x = 1$, with poles marked by dashed vertical lines, as a function of frequency ν ($2t = 1$). The red line shows the exchange-correlation kernel.

Moreover, with only two electrons, the exchange is precisely minus half the Hartree, which has no frequency dependence. Thus the interesting dynamic contribution to the kernel is purely correlation,

$$f_{c,\mathrm{dyn}}(\nu) = (a_s - a)\,\nu_+^2 + \frac{b\,\nu^2}{\nu_+^2 - \nu_f^2}. \qquad (23)$$

This dynamic contribution depends on only three parameters, a, b and ν_f, which are in turn functions of u and $x = \Delta v/2t$. But, by virtue of ground-state DFT, the one-body potential is a unique function of the density (difference), and so the three parameters in the kernel are functions of u and ρ, which is how they appear in a TDDFT calculation. This dependence can be found by using the results of reference [61] for the ground-state, that we summarize in Appendix C.2. In short, a very accurate approximation for the universal contribution to the energy functional, $\mathcal{F}(\rho, u)$, can be found. Since minimizing the ground-state energy yields $x = -\partial\mathcal{F}/\partial\rho$, this is an explicit expression for $x(\rho, u)$. This expression can be inserted into the three parameters to deliver the kernel functional. A comparison between the exact value of $z = x/u$ and the approximation is shown in Figure 3, and any differences are invisible to the eye.

In Figure 4, we plot the response functions and kernel for $u = 1$ and $x = 1$, a relatively weakly correlated and asymmetric system. The exact response function (black) has poles at both the first excitation (ν about 1.4) and the second (about 3.1). The KS function (blue) has only a single pole, corresponding to the KS first excitation,

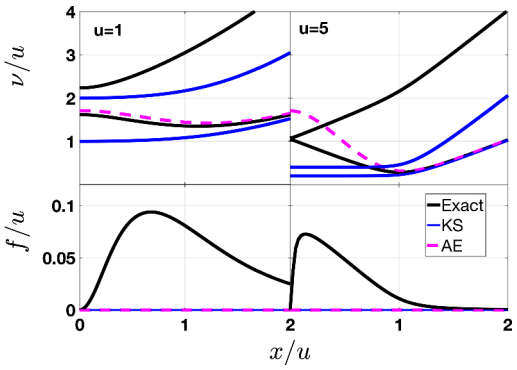

Fig. 5. Transition frequencies (top) and oscillator strength for the many-body system (solid black), its Kohn-Sham counterpart (solid blue) and the adiabatically exact approximation (magenta) as a function of x, for $u = 1$ (weakly correlated regime) and $u = 5$ (strongly correlated regime) ($2t = 1$).

which is close to the exact first excitation because this is a weakly-correlated case. But there is no sign of the second excitation in the KS response. The kernel has its own pole at about 2.95 which, when added to the KS response function, produces the exact second excitation. Note that this requires a pole in the kernel at frequency ν_f: a smooth kernel would not produce the needed pole in χ. Note also that expansions of the parameters in the kernel (in, for example, powers of u) do not yield a well-defined expansion of the kernel itself, as they differ by arbitrarily large amounts for frequencies near the poles.

In almost all applications of TDDFT, the adiabatic approximation is used, i.e., $f_{\mathrm{HXC}}(\nu)$ is replaced by a constant. We define the adiabatically exact (AE) approximation by replacing $f_{\mathrm{HXC}}(\nu)$ with the exact $f_{\mathrm{st}} = f_{\mathrm{HXC}}(0)$ in equation (21). This yields

$$\chi_{\mathrm{AE}}(\nu) = \frac{1}{1/\chi_{\mathrm{S}} - f_{\mathrm{st}}} = \frac{2\,\nu_s\,W_s}{\nu_+^2 - \nu_{\mathrm{AE}}^2}, \qquad (24)$$

where $\nu_{\mathrm{AE}} = \sqrt{\nu_s\,\nu_1\,\nu_2\,W_s/\nu_4}$ is the (single) excitation frequency in the adiabatic approximation. Since the AE approximation has no poles in the kernel, it fails to generate any excitations in the response beyond those in the KS response function, one of its principal failings. In fact, the weight and oscillator strength are identical to the KS values. It is simply that the position of the KS excitations are shifted.

In Figure 5, we show the values of transition frequencies and oscillator strength for both weak (left panel) and strong (right panel) interaction. For $u = 1$ and in the $x/u > 1$ domain for $u = 5$, the KS values are a reasonable approximation to the exact values, and the AE correction greatly improves the first transition frequency. In both cases (KS and AE), $f = 0$, but the exact value of f is never greater than 0.1. On the other hand, for $u = 5$ and $x/u < 1$, the KS single is a vast underestimate relative to the exact single, the AE is a serious overcorrection, the KS double (placed at double the KS single) remains very far from its physical value, and f can be as large as 0.4, i.e., almost half the oscillator strength can

go into the second excitation. In the next subsection we will draw a close analogy between this behavior and that of a real stretched diatomic molecule. Thus a frequency-dependent kernel is vital to produce even qualitatively correct excitations when correlation is strong. Note that although the first excitation improves when $x/u > 1$, and f is also small, the second transition remains very badly described by its KS analog, even for high asymmetry.

When we come to discuss approximations to the dynamical kernel, we will write these in terms of a, b, and ν_f. The corresponding transition frequencies and oscillator strength can be found directly from any such set. Defining $\gamma = (\nu_f^2 + (c+b)/a)/2$, and $\Delta = \sqrt{\gamma^2 - \nu_f^2\, c/a}$, we find:

$$\nu_{1,2}^2 = \gamma \mp \Delta, \quad f = \frac{1}{2}\left(1 - \frac{\nu_f^2 - \gamma}{\Delta}\right). \tag{25}$$

We end this section with a well-known result. In DFT, the fluctuation-dissipation theorem is often cited [74,75], and can be the starting point of RPA-type approximations to the ground-state XC energy. In Appendix B.2, we show

$$E_{\rm XC}(\rho) = -\frac{U}{2}\int_0^1 d\lambda \int_0^\infty \frac{d\omega}{2\pi}\,{\rm Im}\,\chi(\lambda U, \rho, \omega) - \frac{U\,N}{2}. \tag{26}$$

This applies for either $N = 1$ or 2. Here λ multiplies U everywhere, but ρ is kept fixed. This adiabatic connection is the DFT equivalent of the coupling constant. At $\lambda = 1$, one gets the fully interacting system, while at $\lambda = 0$, the KS system is recovered, and $\chi^{\lambda=0} = \chi_s$. Inserting our χ from equation (10), we find a very simple form:

$$E_{\rm XC}(\rho) = -\frac{U}{2}\int_0^1 d\lambda \left(\sum_{i=1}^{2} W_i(\lambda U, \rho) - N\right), \tag{27}$$

an elegant expression of the ground-state XC energy in terms of the weights of the excitations.

3.4 Matrix formulation

The analog of the TDDFT matrix equation (3) for the Hubbard dimer is particularly simple due to the small Hilbert space. We can derive this from equation (21), with the observation that $\chi(\nu)$ has a pole at the exact interacting frequencies $\nu_{1,2}$ (Eq. (10)), and so $\chi^{-1}(\nu_{1,2}) = 0$. Then, inverting equation (18) for $\chi_{\rm S}^{-1}(\nu)$ on the right-hand-side of equation (21), and rearranging to solve for ν, we obtain [49]

$$\nu^2 = \nu_{\rm S}^2 + 2\nu_{\rm S} W_{\rm S} f_{\rm HXC}(\nu) \equiv R_{\rm H}(\nu), \tag{28}$$

whose solutions yield the exact frequencies of the interacting Hubbard dimer, ν_1, ν_2. This is the analog of what is known as the small matrix approximation for real molecules, when the matrix R of equation (3) is truncated to just one single KS excitation. Since there is only one KS single excitation in the Hubbard dimer, equation (28) is exact.

As discussed in Section 2.1, oscillator strengths of real molecules are extracted from eigenvectors of the TDDFT linear response matrix equation (3). To obtain the oscillator strengths of the exact transitions in the Hubbard dimer from equation (28), we retrieve a formula from reference [4], which showed that the eigenvectors G_I of the matrix equation (3) must be first normalized such that

$$G_I^\dagger \left(1 - \left.\frac{\partial R}{\partial \omega^2}\right|_{\omega_I}\right) G_I = 1\,, \tag{29}$$

before the oscillator strengths can be correctly extracted. Since usually an adiabatic approximation is used, there is no frequency-dependence in the matrix R and so this condition just reduces to requiring normalized eigenvectors. In fact, to our knowledge, there has not been any use of this result of reference [4] in the literature, likely because of the predominance of the adiabatic approximation. However, with a non-adiabatic kernel, such as we have in the Hubbard dimer, the frequency-dependence results in a rescaling of the eigenvectors, redistributing the oscillator strength in a way that depends on the excitation frequency. For our Hubbard dimer, this means the oscillator strength from the single KS excitation gets split into two, according to

$$G_{1,2} = \frac{1}{\sqrt{1 - \left.\frac{\partial R_{\rm H}(\nu)}{\partial \nu^2}\right|_{\nu_{1,2}}}}. \tag{30}$$

Taking the derivative of equation (28), using equations (18) and (10) in equation (21), then readily gives us

$$G_i^2 = \frac{\nu_i W_i}{\nu_{\rm S} W_{\rm S}}\,. \tag{31}$$

That is, the ratio of the transition strength of the second excitation to the total transition strength, is

$$\frac{G_2^2}{G_1^2 + G_2^2} = \frac{\nu_2 W_2}{\nu_1 W_1 + \nu_2 W_2}\,, \tag{32}$$

coinciding with our definition of f in equation (13).

4 Weak and strong correlation

4.1 Background

Here we study the behavior of the system when interaction is weak, i.e., $u \lesssim 1$. Of course, all quantities (excitation energies, oscillator strengths, kernel parameters, etc.) can be expanded as a power series in u, and the results are given in Appendix C.3. But we make a note of caution here: There are many different expansions in powers of u. They differ in terms of which variable is held fixed. From a many-body point of view, the natural expansion is holding the external potential $x = \Delta v/2t$ fixed, and expanding in powers of u, which is the meaning we have used so far.

However, even in ground-state DFT, the natural expansion is the one used in the adiabatic connection formula, in which Δn is held fixed. This expansion differs from the many-body one. As we will show later, when dealing with strong correlation, even in many-body theory, it will be more useful to hold the ratio $z = x/u$ fixed than keeping x fixed.

A second crucial point is that, in any of these expansions, because of the frequency-dependence in the kernel and the existence of a pole, there is no simple connection between an expansion of the kernel parameters and the resulting behavior of calculated transition frequencies. Expansions in powers of u do not commute with expansions in terms of the frequency, say. It has long been known that, evaluating the kernel to leading order in λ, i.e., at the exchange level, yields transitions that contain *all orders* in λ, due to the non-linearity of the RPA-type equation. Thus, use of the exchange kernel leads to approximate correlation corrections to the transitions.

4.2 Relation to dressed TDDFT

In the weak interaction limit the true excitations have a clear single and double excitation character respectively. Here we discuss some similarities and differences to dressed TDDFT. First, dressed TDDFT isolates a single- and double-excitation from among a spectrum of many excitations, assuming they are more strongly coupled to one another than to any other. Here, there are only these two excitations in the entire spectrum. This is why the the exact kernel of equation (23) has a simple pole of the same type introduced in dressed TDDFT. The only difference is that there are two poles here, $\pm\nu_f$, which reflects the symmetric inclusion of both forward and backward transitions. However, the essential condition of dressed TDDFT, namely that a specific single excitation is closest and most strongly coupled only to a specific double excitation, is not satisfied here. For example, in the weak coupling limit, the double is at twice the frequency of the single, and no closer to it than the ground-state is.

4.3 Weak-correlation kernel

To create an approximation that is appropriate for conditions of weak correlation (corresponding to most current successful applications of lrTDDFT), we expand in small u for a fixed value of x. We consider the many-body expansion of Appendix C.3 in which we keep terms up to order u^2 in each of the parameters determining the kernel:

$$
\begin{aligned}
a^{WC2} &= \frac{p_0}{4}\left(1 - x^2\,\tilde{u} + \frac{(1+8\,x^2)\,\tilde{u}^2}{8}\right),\\
b^{WC2} &= \frac{9\,x^2\,p_0^3\,\tilde{u}^2}{16}\left(1 - \frac{2\,p_0^2\,\tilde{u}}{3}\right),\\
\nu_f^{WC2} &= 2\,p_0\left(1 + \frac{p_0^2\,\tilde{u}^2}{8}\right),
\end{aligned}
\tag{33}
$$

where $p_0 = \sqrt{1+x^2}$ and $\tilde{u} = u/p_0^3$, plus an extra term in the expansion of b. With these expressions, we study the weakly correlated behaviour of the dimer.

In Figure 6 we plot the deviations of the transitions from their KS values $\Delta\nu_j = \nu_j - j * \nu_s$, $j = 1, 2$, both exactly and for the AE and weakly-correlated approximations for $u = 1$ and $u = 2$. We see that, in the weakly correlated case ($u = 1$ or less), the adiabatic approximation for the transition frequencies is very close to the exact quantity for both cases. This is what is used (usually with a ground-state approximation) in most applications of TDDFT. However, here we can also add the dynamical correction, expanded to leading order in the strength of the correlation, and we find it improves the results even further. This is especially apparent for the oscillator strength, where the performance is very good, as $u = 1$ is no longer very weak correlation. However, once u is large enough, this approximation must fail. The weakly correlated approximation delivers poor results for the frequencies and the oscillator strength for $u = 5$, except for $\bar{x} = x/\sqrt{1+x^2}$ close enough to one. We explore this point in the next section.

However, these are *not* explicit functionals of the density, but rather they are post-calculation corrections to a standard TDDFT calculation with an adiabatic kernel. To convert them to density functionals, we express x as a function of ρ by using the relationship $x = -\partial f/\partial\rho$ and the ground-state density functional $\mathcal{F}(\rho, u)$ described in Appendix C.2. We expand the functional in powers of u as described in Appendix C.2.1 and find

$$
x \simeq \frac{\rho}{r} + \rho\,u + \frac{5}{8}\,\rho\,r^3\,u^2 + \frac{1}{4}\,\rho\,r^2\,\left(1 - 4\,\rho^2\right)\,u^3, \tag{34}
$$

where $r = \sqrt{1-\rho^2}$. This is then used to eliminate x in equations (33) power by power, yielding:

$$
\begin{aligned}
a^{\mathrm{WC2}}(\rho) &= \frac{1}{4\,r}\left(1 + \frac{1}{8}\,r^4\,u^2\right),\\
b^{\mathrm{WC2}}(\rho) &= \left(\frac{3\,\rho\,r}{4}\right)^2 u^2\left(1 + \frac{4}{3}\,r\,(1 - 3\,\rho^2)\,u\right),\\
\nu_f^{\mathrm{WC2}}(\rho) &= \frac{2}{r} + 2\,\rho^2\,u + \frac{1}{4}\,r^3\,(1 + 9\,\rho^2)\,u^2.
\end{aligned}
\tag{35}
$$

4.4 When is a system strongly correlated?

In this section, we discuss the concept of strong correlation in the context of density functional theory, with special emphasis on the differences from many-body theory. The key point is that, because the exact KS system reproduces the exact density of the system, even when correlations are strong, it can be a much closer mimic of the true system than the traditional many-body starting point, namely a self-consistent Hartree-Fock approximation, depending on what property is of interest. For example, when correlations are strong, the lowest-energy self-consistent HF approximation breaks spin symmetry (the unrestricted solution, UHF), whereas the KS wavefunction always remains a singlet, no matter how strong correlation is (using the exact ground-state functional).

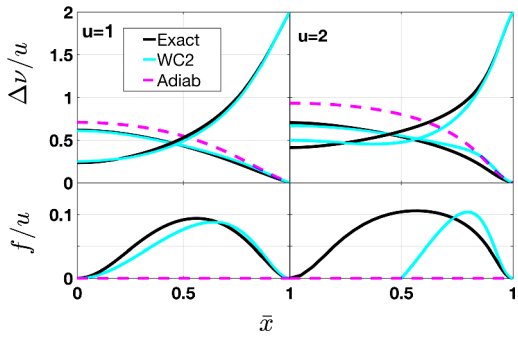

Fig. 6. Corrections to KS transition frequencies and oscillator strength as a function of $\bar{x} = x/\sqrt{1+x^2}$ for exact system (solid black), within AE approximation (dashed magenta) and with the weak-correlation dynamical approximation WC2 of equation (33) (solid cyan).

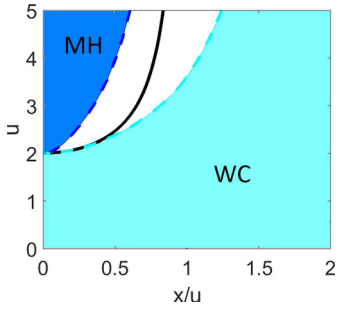

Fig. 7. Physical regimes in the Hubbard dimer: dark blue is the pure Mott-Hubbard regime (limited error of approximations around MH limit), while pale blue is the pure weakly correlated regime (limited error of approximation about the WC limit). The solid black line is the contour of 86% overlap between the many-body and Kohn-Sham wavefunctions.

Thus the greatest differences occur just as correlations become strong.

The first issue to address is how to decide when our dimer is strongly correlated. The most studied case is the symmetric case ($x = 0$). Here, it is clear that a Taylor expansion in small u has a radius of convergence of $u = 2$ (branch cut at $u = 2i$), while a similar expansion in $1/u$ also converges up to $1/2$. Thus $u = 2$ is very definitively the dividing point between weak and strong correlation.

But DFT is primarily concerned with inhomogeneous systems, which for our dimer means asymmetry, so our definition must be generalized to all values of x. When the potential is highly asymmetric, does this categorization change? In fact, it does so, in an extremely important fashion.

In Figure 7, we plot a contour of the square overlap of the exact ground-state KS wavefunction with the exact interacting wavefunction as a function of $\bar{z}$ and $\bar{u}$. We have chosen the value $\sqrt{3}/2 \approx 0.86$, as this yields precisely $u = 2$ ($\bar{u} = 1/\sqrt{2}$) when $x = 0$. We have also colored in the region where Mott-Hubbard physics dominates (dark blue) and the region where weak correlation approximations work (pale blue). These will be quantified below. For now, the important lessons of Figure 7 are first that

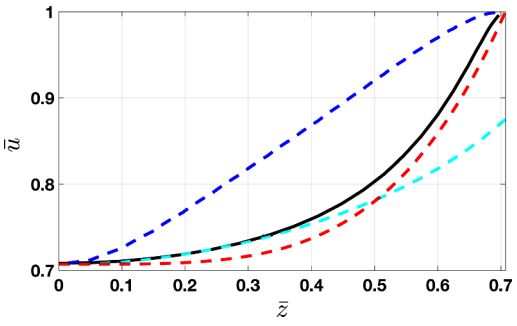

Fig. 8. Contour plot of the square of the overlap between the true and KS wavefunctions (black), as well as contours of error for WC2 (cyan) and MH approximations (blue), and our simple interpolation (red line).

most of the phase diagram is colored pale blue and second that the variable on the x-axis is x/u, i.e., the asymmetry divided by the interaction. In fact, if this ratio is greater than 1, the dimer is always weakly correlated, i.e., the black borderline never crosses $x = u$, no matter how strong the interaction. (The edge of the pale blue region simply delineates a contour of finite error for the WC approximation, as described below.) This is because, in the ground state, both electrons sit on one site, despite the strength of the interaction.

4.5 Mott-Hubbard regime and expansions

To capture the physics described above, we introduce a new variable

$$z = \frac{x}{u} = \frac{\Delta v}{U}. \tag{36}$$

This is the onsite potential difference, but measured on the scale of the interaction. We show below that this is a more useful variable than x in considering strong correlation. A similar variable was used in reference [76] in their analysis of a Hubbard model of LiF. We also define the reduced variables,

$$\bar{u} = \frac{u}{\sqrt{4+u^2}}, \qquad \bar{z} = \frac{z}{\sqrt{1+z^2}}, \tag{37}$$

that run from zero to one as u and x span their whole range from zero to infinity. Here, $u = 2$ corresponds to $\bar{u} = 1/\sqrt{2}$, while $x = u$ corresponds to $\bar{z} = 1/\sqrt{2}$.

Figure 8 replots Figure 7 in terms of the reduced variables, and with more detail. The solid black line is still the 86% overlap contour. For $\bar{u}$ below this contour, the overlap is at least this value, and we consider the system weakly correlated. The first thing to notice is that the contour is confined to the upper left corner of the $\bar{u}$–$\bar{z}$ plane. In all the remaining phase space, the overlap is better than 0.93, including all $\bar{z} > 1/\sqrt{2}$ (e.g., $x > u$), *no matter how large the value of* u. It makes intuitive sense that for sufficiently asymmetric systems, u must be much larger to create strong correlation effects. What is notable is that the system is always weakly correlated when $x > u$. This

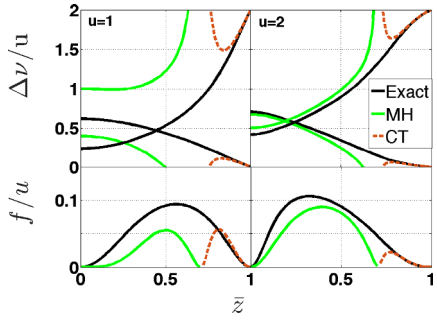

Fig. 9. Corrections to KS transition frequencies and oscillator strength as a function of $\bar{z} = z/\sqrt{1+z^2}$ for exact system (solid black) and with the MH2 (solid green) and CT (dashed brown) expansions.

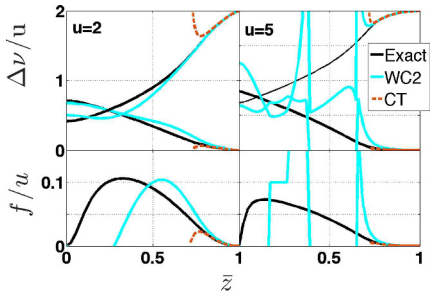

Fig. 10. Corrections to KS transition frequencies and oscillator strength as a function of $\bar{z}$ exactly (black), WC2 (cyan) and CT expansion (dashed brown).

is the explanation for the success of our weakly-correlated kernel to the right in the previous figures.

Now, the upper left corner (large u, small x) is the Mott-Hubbard regime, i.e., the familiar physics of strong correlation in the symmetric limit. In this quadrant, the strong-correlation expansion described below is accurate. Above the blue contour, the strong correlation expression for the ground state energy has an error of 0.23 at most (in units of $2\,t$). On the other hand, below the cyan contour, the WC2 approximation for the energy has an error of only 0.086 at most (in units of $2\,t$ again). The overlap contour runs neatly between these two. Thus we need only the weakly-correlated and the MH regimes to cover all the physics in the dimer. We can make a simple smooth interpolation to capture the contour, namely

$$\bar{u}_c(z) = a + b\bar{z}^p, \tag{38}$$

where a and b are positive real numbers, and p a positive integer. We find $p = 4$ simulates the actual contour well. Then $a = 1/\sqrt{2}$ and $b = 4(1-a)$ to achieve the correct limits. This approximate contour is also plotted in Figure 8.

So, in order to capture the MH regime, we perform an expansion for large u, keeping z fixed and less than 1. The results are (Appendix C.4)

$$\begin{aligned} a^{\mathrm{MH2}} &= \frac{u\,z_a}{8}\left(1+\frac{2\,(1+z^2)}{z_a^2u^2}\right),\\ b^{\mathrm{MH2}} &= \frac{u^3\,z^2\,z_a^2}{2\,z_b}\left(1+\frac{7\,z^4+18\,z^2-1}{z_a^2\,z_b u^2}\right),\\ \nu_f^{\mathrm{MH2}} &= u\,z_b^{1/2}\left(1-\frac{z^2-2}{z_a\,z_b u^2}\right), \end{aligned} \tag{39}$$

where $z_a = 1-z^2$ and $z_b = 1+3\,z^2$. Clearly, these expressions fail for $z = 1$ or larger, with higher-order terms diverging. The complementary expressions for $z > 1$ are the CT approximation, and are given in the same Appendix.

Figure 9 shows the exact deviations from the KS frequencies and oscillator strength alongside the MH and CT approximations. For larger u, MH works well until close to $x = u$, and CT works beyond that. But clearly, near $z = 1$, neither work well, and in fact diverge. The region in which this failure occurs shrinks with increasing u, but always exists. For smaller u, such as $u = 1$, this region is so large that the MH approximation essentially never works, and CT only works for very large z.

In Figure 10, we compare the performance of the WC2 and CT expansions. For $u = 2$ (left panel) and smaller, it is clear that WC2 is about the same as CT for large z, but works much better for smaller z. Even for $u = 5$, where WC2 fails badly for $z < 1$, it still works better than CT for $z > 1$. In fact, we found no region in parameter space where CT outperformed WC2. This is consistent with the contours of Figure 8.

4.6 Interpolation kernel

In this section, we construct an interpolation kernel between the MH and WC regimes. We first improve the weakly correlated and MH approximations so that they match as smoothly as possible in the crossover region. We define WC4 as the expansion of the dynamic kernel parameters (a, b, and ν_f) to 4th order in u, for fixed x. The corrections to WC2 (Eq. (33)) are:

$$\begin{aligned} \Delta a^{\mathrm{WC4}} &= \frac{p_0\,\tilde{u}^3}{16}\left(x^2\,(4\,x^2-1)+\frac{16\,x^4\,(8\,x^2-9)-1}{32}\,\tilde{u}\right),\\ \Delta b^{\mathrm{WC4}} &= \frac{p_0^3\,x^2\,(8\,x^4+58\,x^2+23)}{128}\,\tilde{u}^4,\\ \Delta\nu_f^{\mathrm{WC4}} &= \frac{p_0^3\,\tilde{u}^3}{4}\left(x^2+\frac{16\,x^4-9\,x^2-1}{16}\,\tilde{u}\right). \end{aligned} \tag{40}$$

We see in Figure 11 that these clearly improve the frequencies and oscillator strength over WC2. On the other hand, while adding one or two further terms in the MH expansion does not seem to improve matters much, removing divergences at $x = u$ does improve things. We can regularize the MH2 expressions by replacing $u\,z_a$ with $\sqrt{u^2\,z_a^2+z^2}$. This provides a significantly smoother matching with the WC4 approximation at the crossover region when the interpolation scheme explained below is deployed. Figure 11 shows the impact of these two schemes on the frequencies and oscillator strength, where we use equation (40) for the weak-coupling expansion and (a regularized) equation (39) for the MH expansion. For $u = 5$,

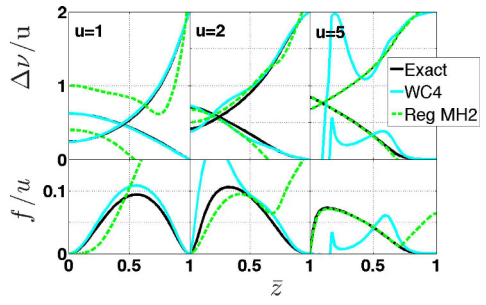

Fig. 11. Corrections to KS transition frequencies and oscillator strength as a function of $\bar{z}$ exactly (black), weakly correlated expansion WC4 (cyan) and regularized MH2 expansion (green).

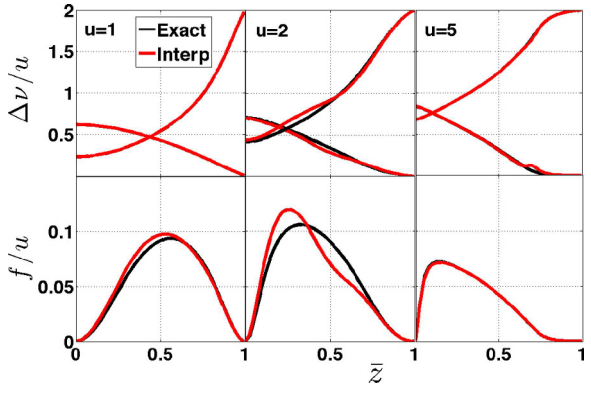

Fig. 12. Exact (solid black) and interpolated (red) deviations from KS frequencies and oscillator strength as a function of $\bar{z}$.

we clearly see (regularized) MH working well up to $x = u$, and WC4 working well beyond that (and each one failing outside its domain). As u is reduced, the regime where WC4 fails shrinks ($u = 2$), until for $u = 1$, WC4 is almost perfect everywhere.

We suggest the following interpolative scheme for each of the kernel parameters:

$$a_{\rm int}(u,z) = n_F\, a^{\rm WC4}(u,z) + (1-n_F)\,\tilde{a}^{\rm MH2}(u,z), \quad (41)$$

where the tilde indicates that MH2 has been regularized, and $n_F(u,z)$ varies smoothly from 1 to 0 as the contour $u_c(z)$ given by equation (38) (and shown in Fig. 8) is crossed. We choose a Fermi function:

$$n_F(u,z) = \frac{1}{e^{\beta(u-u_c(z))}+1}. \quad (42)$$

We find $\beta = 20$ yields a reasonably accurate transition.

We plot the results of the interpolation kernel for several values of u as a function of z in Figure 12. We see that it works reasonably well for $u < 1$ for all x, and for $z > 1$ ($\bar{z} > 1/\sqrt{2}$) for any u, and gives an imperfect but reasonable interpolation in between. This approximate kernel is not designed to yield the extreme accuracy of the ground-state approximations of reference [61], but just to show that once the limiting physics is included, an approximation can be generated that works reasonably in

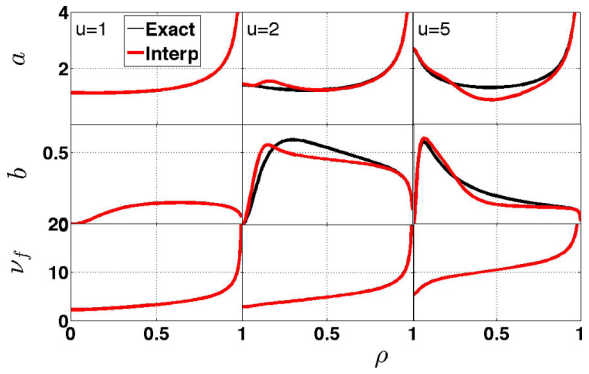

Fig. 13. Exact (solid black) and interpolated (red) kernel parameters as a function(al) of density ρ. The parameter b for $u = 5$ has been divided by 10 to fit in the same y-scale as in the other two panels.

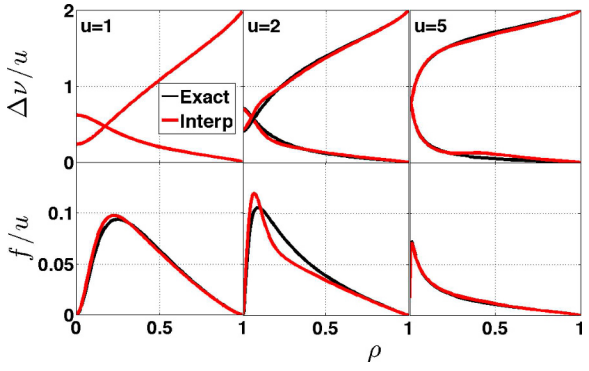

Fig. 14. Exact (solid black) and interpolated (red) frequency deviations and oscillator strength as a function of density ρ.

all regimes. Its limitations are most easily understood by starting with $u = 5$, where the error in the stitching is visible at $\bar{z} = 1/\sqrt{2}$ (i.e., $z = 1$, or $x = u$), but it is small and spans a relatively small region of z. As u is reduced, this region grows, and is largest for $u = 2$. By the time $u = 1$, this region has vanished entirely, and the WC4 formula dominates and works well everywhere.

The final step is to write these interpolations as a function of u and ρ instead of the dependence on x through $\bar{z}$. This is accomplished again using the results for the $\mathcal{F}$-functional from Appendix C.2. We thus find $z = x(\rho,u)/u = -1/u \times \partial f/\partial\rho$. The values of $z(\rho,u)$ can be inserted into equation (41) to deliver the kernel functional. The kernel parameters as a function(al) of ρ are plotted in Figure 13. The frequency deviations and oscillator strength as a function of ρ are plotted in Figure 14.

5 Discussion and outlook

5.1 Analogy to real diatomic molecules

The asymmetric Hubbard dimer behaves similarly to real diatomic molecules stretched to large bond-lengths when the latter are treated within a "minimal model", i.e.,

when only the KS HOMO and LUMO orbitals are considered. If the molecule is neutral, these two orbitals become energetically so close when approaching the dissociation limit, that the minimal model captures the essential physics since couplings to the many other orbitals in the molecule are far smaller in comparison. In the Hubbard model, there are only ever two orbitals, so it makes a natural model for these stretched molecules. (Such a minimal model does not capture van der Waal's interactions between the atoms, which result from fluctations within each atom.) The problem of laser-induced charge-transfer dynamics has been studied in this way [20,49,50]. Here we compare the kernel of the real molecule in this limit with that of the Hubbard model.

The ground state of such a stretched neutral molecule has close to one electron on each atomic HOMO. Assuming then that the atomic orbitals are orthogonalized, we consider the MH limit of the Hubbard dimer, whose ground state is (see Appendix C.5 for details)

$$|\psi_0\rangle \approx \frac{1}{\sqrt{2}}\left(|12\rangle + |21\rangle\right). \tag{43}$$

(On the other hand, a stretched cationic diatomic molecule approaches the CT limit of the Hubbard dimer, in the particular case where the LUMO and HOMO of the molecule are on different atoms.) In neutral molecules, the exact KS HOMO has the form of a bonding orbital, straddling both atoms with a density equal to the sum of the individual atomic HOMO densities, while the LUMO has approximately an antibonding form. This holds for both homo-atomic and hetero-atomic neutral molecules [19,77]. Their orbital energies become increasingly degenerate as the molecule is stretched, so the KS excitation energy becomes very small (exponentially small with the interatomic distance R). This is consistent with the Hubbard dimer, where this excitation energy is equal to the hopping integral $2\,t$, which would also decay exponentially with R (see again Appendix C.5). Strictly speaking, to model a heteronuclear neutral molecule with a Hubbard dimer, we should require different U-parameters on each site, with $U_i = I_i - A_i$ (although Appendix B.3 shows how to map such a dimer onto one with the same U on each site). In any case, even with the same U on each site, we capture the basic qualitative features of excitations and the xc kernel of stretched molecules with the MH limit of the Hubbard dimer.

For the molecule, we can write the kernel (in the minimal model, restoring dimensional units) [19,20] as $f^{qq}_{\rm HXC}(\omega) = f^{qq}_{\rm HXC}(\omega = 0) + f^{qq}_{\rm HXC,dyn}(\omega)$. The adiabatic part

$$f^{qq}_{\rm HXC}(\omega = 0) = \frac{\omega_1\omega_2}{4\omega_{\rm S}} - \frac{\omega_{\rm S}}{4}, \tag{44}$$

where $\omega_1 = I_b - A_a - 1/R$, $\omega_2 = I_a - A_b - 1/R$ are the excitation frequencies for charge-transfer excitations from atom b to atom a and vice-versa, and $\omega_{\rm S} \sim e^{-\alpha R}$ is the Kohn-Sham HOMO-LUMO gap. Comparing with the adiabatic Hubbard kernel in the MH limit, equation (22),

$$f_{\rm st} = \frac{\nu_1\,\nu_2}{2\,\nu_4} - \frac{\nu_{\rm S}}{2\,W_s}, \tag{45}$$

we see the adiabatic part in both is proportional to the product of the exact excitation frequencies, and both blow up as in the limit (u/x or $R \to \infty$). Comparing the dynamical part

$$\begin{aligned} f^{qq,{\rm dyn}}_{\rm HXC}(\omega) &= f^{qq}_{\rm HXC}(\omega) - f_{\rm HXC}(\omega = 0) \\ &= \frac{\omega^2}{\omega_{\rm S}}\left(\frac{\delta^2}{\omega^2 - \omega_1\omega_2}\right), \end{aligned} \tag{46}$$

where $\delta = (\omega_1 - \omega_2)/2$, with that of the dimer, equation (23), we observe both have a pole at the product of the two exact excitation frequencies, and both blow up in the limit. Thus the kernel in the case of a stretched diatomic molecule maps closely to the form of the kernel for the Hubbard dimer in the MH limit (Appendix C.5).

5.2 Applications

In this paper, we have thoroughly explored the linear response TDDFT of the Hubbard dimer. We have shown how the standard expansion of many-body theory is not useful for understanding the competition between inhomogeneity effects and correlation effects. We find that strong correlation is better characterized by an expansion in which the ratio $\Delta v/U$ is kept fixed rather than Δv itself. It makes sense that inhomogeneity should be measured relative to the interaction strength. By expanding in powers of $1/u$ keeping that ratio fixed, we find an accurate expansion for the strongly correlated limit. Moreover, we can smoothly interpolate this expansion with the standard weakly-correlated limit, and construct an explicit approximate XC kernel that works well in both regimes, and does not fail badly in between.

How can this kernel be used? Clearly, this kernel itself is constructed within a lattice model, and so might be used as an approximation (or the starting point of a more general approximation) to apply TDDFT to lattice models. There is substantial history of studies in this area [40–56,60]. Such applications can be useful in studying systems too large to be accessible by more direct quantum solvers, where the relative inexpensiveness of DFT can be crucial.

A second way one could imagine this kernel being used is in a continuous real-space calculation, e.g., a diatomic molecule, in which some choice has been made that assigns some fraction of the electrons to each atom. Then the kernel might be applied directly to these occupation numbers, allowing double excitations to be included in TDDFT calculations of the system. This might prove particularly effective when the bond is stretched, so that electrons truly are localized on each site.

A third way the kernel might be used is simply as an illustration of the effects of strong-correlation within linear-response TDDFT, to inspire construction of frequency-dependent kernels that can be applied to realistic systems. Such kernels, when applied within a minimal

basis model, should capture the same effects shown here, as discussed in the previous section.

The range of validity of the kernel can be extended and tested by solving larger or more complex systems like multi-orbital Hubbard dimers, because some of these models are amenable to numerically exact solutions.

An important point in this work is also the literal existence of the kernel itself. We have given the explicit frequency-dependence of the dynamic XC kernel that is exact for this Hamiltonian and two electrons. Such kernels do exist and reproduce the exact transition frequencies and oscillator strength, including that of the double excitation, even when it represents a charge transfer.

The Hubbard dimer can be easily generalized to the asymmetric Anderson dimer as discussed in Appendix B.3. So the results presented here can be applied to this later model.

We have also proven or illustrated many smaller, related results, such as how to identify multiple excitations from single ones, the oscillator strength sum-rule for this lattice model, the adiabatic connection formula and the Kohn-Sham linear response for fractional occupations.

DC and JF wish to thank funding support from the Spanish Ministerio de Economía y Competitividad via grant FIS2012-34858. NTM thanks the US National Science Foundation CHE-1566197 for support. KB acknowledges DOE grant number DE-FG02-08ER46496. All the authors have benefitted either directly or indirectly from the accumulated impact of Prof. Gross's works. Some also acknowledge about 45 accumulated years of friendship and learning at the feet of Prof. E.K.U. (Hardy) Gross, who taught us (almost) everything we know about time-dependent density functional theory. We hope that this small contribution, demonstrating the exactness of TDDFT in the simplest possible case, might contribute to elucidating how the theory works to skeptics in many-body theory or ab-initio computational chemistry. While this paper (and, indeed, much of Prof. Gross's work) might be regarded as FEPU (formally exact, practically useless), the proof of the RG theorem [1] was clearly anything but.

Author contribution statement

All authors have contributed to the article.

Appendix A: Exact energies and weights

We use the following basis states to span the sub-space labelled by $N = 2$, $S^2 = 0$ and $S_z = 0$:

$$\begin{aligned} |\varphi_a\rangle &= \frac{|12\rangle + |21\rangle}{\sqrt{2}} = (1,\,0,\,0)^\dagger, \\ |\varphi_b\rangle &= |11\rangle = (0,\,1,\,0)^\dagger, \\ |\varphi_c\rangle &= |22\rangle = (0,\,0,\,1)^\dagger. \end{aligned} \tag{A.1}$$

A.1 Many-body states

The three singlet eigen-energies of the Hubbard dimer within the sub-space are ($i = 0, 1, 2$):

$$\begin{aligned} e_i &= \frac{2}{3}\left(u + \sqrt{3 + 3\,x^2 + u^2}\,\cos\left(\theta + \frac{2\,\pi}{3}\,(i+1)\right)\right), \\ \theta &= \frac{1}{3}\,\cos^{-1}\left[\frac{9\,x^2 - 9/2 - u^2}{(3 + 3\,x^2 + u^2)^{3/2}}\,u\right], \end{aligned} \tag{A.2}$$

and $\cos^{-1}$ denotes the principal value of the complex arccos function. Next, the eigenstates are,

$$\begin{aligned} |\Psi_i\rangle &= (\alpha_i,\,\beta_i^+,\,\beta_i^-)^\dagger, \\ \alpha_i &= \frac{e_i - u}{e_i\,r_i}, \quad \beta_i^\pm \frac{u - e_i \pm x}{\sqrt{2}\,r_i}, \\ r_i = r(e_i) &= \sqrt{x^2 + (e_i - u)^2\,(1 + 1/e_i^2)}. \end{aligned} \tag{A.3}$$

Notice that normalization implies $|\alpha_i|^2 + |\beta_i^+|^2 + |\beta_i^-|^2 = 1$, and that the density for each of the three states is $\rho_i = \Delta n_i/2 = (\beta_i^+)^2 - (\beta_i^-)^2$. We denote the ground-state density $\Delta n = \Delta n_0$ (or $\rho = \rho_0$) and the transition frequencies as

$$\begin{aligned} \nu_1 &= e_1 - e_0 = 2\,\sqrt{1 + x^2 + u^2/3}\,\sin\theta, \\ \nu_2 &= e_2 - e_0 = 2\,\sqrt{1 + x^2 + u^2/3}\,\sin(\theta + \pi/3). \end{aligned} \tag{A.4}$$

The weights are given by

$$\sqrt{W_{1,2}} = |\langle\psi_0|\Delta\hat{n}|\psi_{1,2}\rangle| = \frac{4\,x\,e_{2,1}}{r(e_0)\,r(e_{1,2})}, \tag{A.5}$$

while

$$\nu_3 = \nu_1\,W_1 + \nu_2\,W_2 = -\frac{8\,(e_0 - u)^2}{e_0\,r_0^2}. \tag{A.6}$$

Equations (A.4) and (A.5) are used in equation (11), and equation (A.6) is used in equation (12) of the main text.

A.2 Kohn-Sham states

The spin-independent dimensionless Hamiltonian written in the single-particle $\{|1\rangle, |2\rangle\}$ basis is

$$\hat{h}_s = \begin{pmatrix} \frac{\bar{v}_s}{2\,t} - \frac{\Delta v_s}{4t} & -1/2 \\ -1/2 & \frac{\bar{v}_s}{2\,t} + \frac{\Delta v_s}{4t} \end{pmatrix}, \tag{A.7}$$

where the KS potentials are

$$\begin{aligned} \bar{v}_s &= \bar{v} + \bar{v}_{\rm Hxc} = \bar{v}_{\rm Hxc}, \\ \frac{\Delta v_s}{2t} &= \frac{\Delta v}{2t} + \frac{\Delta v_{\rm Hxc}}{2t} = x_s = x + x_{\rm Hxc}. \end{aligned} \tag{A.8}$$

It is useful to define the auxiliary variables $r_s = \sqrt{x_s^2+1}$, $\bar{x}_s = x_s/r_s$. Then, the eigenvalues and normalized eigenfunctions are given by

$$e_s^{\pm} = \bar{v}_s/(2\,t) \pm r_s/2, \;\; |\phi^{\pm}\rangle = c_s^{\pm}\,|1\rangle \mp c_s^{\mp}\,|2\rangle, \qquad \text{(A.9)}$$

where $c_s^{\pm} = \sqrt{(1 \mp \bar{x}_s)/2}$. The ground-state density is

$$\rho = \langle\phi_0|\frac{\Delta\hat{n}}{2}|\phi_0\rangle = \bar{x}_s, \;\; x_s = \frac{\rho}{\sqrt{1-\rho^2}}. \qquad \text{(A.10)}$$

The singlet KS 2-particle states can be found from slater determinants of the KS single-particle states:

$$|\Phi_0\rangle = \left(\sqrt{2}\,c_s^+\,c_s^-,\,(c_s^-)^2,\,(c_s^+)^2\right)^{\dagger},$$
$$|\Phi_1\rangle = \left((c_s^+)^2 - (c_s^-)^2,\,\sqrt{2}\,c_s^+\,c_s^-,\,-\sqrt{2}\,c_s^+\,c_s^-\right)^{\dagger}, \qquad \text{(A.11)}$$
$$|\Phi_2\rangle = (\sqrt{2}\,c_s^+\,c_s^-, -(c_s^+)^2,\,-(c_s^-)^2)^{\dagger}. \qquad \text{(A.12)}$$

The KS transition frequencies are:

$$\nu_s = r_{\rm S}, \qquad \nu_d = 2\,r_{\rm S}, \qquad \text{(A.13)}$$

where ν_d is the KS double, trivially twice the single, ν_s. The weights are

$$\sqrt{W_s} = |\langle\Phi_0|\Delta\hat{n}|\Phi_1\rangle| = \frac{\sqrt{2}}{r_s}, \qquad \text{(A.14)}$$

while W_d vanishes entirely. Equations (A.10), (A.13) and (A.14) are used in equation (19) of the main text.

Appendix B: Proofs and generalizations

B.1 Oscillator strength sum rule

The sum rule for the density-density response operator can be obtained from:

$$\langle\Psi_0|\left[\hat{\rho},\left[\hat{\rho},\frac{\hat{H}}{2\,t}\right]\right]|\Psi_0\rangle = -2\sum_{m\neq 0}\nu_m\,|\langle\Psi_0|\,\hat{\rho}\,|\Psi_m\rangle|^2. \qquad \text{(B.1)}$$

Some little algebra shows that the commutators can be written as $\hat{T}/(2\,t)$, yielding

$$\sum_{m\neq 0}\nu_m\,|\langle\Psi_0|\,\hat{\rho}\,|\Psi_m\rangle|^2 = -\frac{1}{2}\,\langle\Psi_0|\,\frac{\hat{T}}{2\,t}\,|\Psi_0\rangle. \qquad \text{(B.2)}$$

This result is general and valid for the Hubbard dimer irrespective of the number of electrons. The relation between the kinetic energy and the weights of the density-density linear response in the Hubbard model has been already established in the literature in the past (see e.g., [71,72]). In these references it is emphasized that the sum rule for this model is not providing the full story because the Hamiltonian contains only a single state per site and thus allows only intraband transitions. The complete f-sum rule includes all allowed interband transitions and does not depend on the electron-electron interaction unlike the case in the Hubbard model [72]. Equation (B.2) reads explicitly for $N = 2$

$$\nu_3 = \nu_1\,W_1 + \nu_2\,W_2 = -\frac{8\,(e_0-u)^2}{e_0\,r_0^2}, \qquad \text{(B.3)}$$

where the right-hand side of the equation is a function of x and u. Equation (B.3) is used in equation (12) of the main text.

B.2 Fluctuation-dissipation theorem

We start by rewriting the Hubbard interaction term in terms of N and Δn,

$$\hat{V}_{ee} = \frac{U}{4}\,(\hat{N}^2 + \Delta\hat{n}^2) - \frac{U\,\hat{N}}{2}, \qquad \text{(B.4)}$$

where we have used the fact that $\hat{n}_{i\sigma}^2 = \hat{n}_{i\sigma}$ for fermion operators. Using this definition we can write the Hamiltonian

$$\begin{aligned}\hat{\mathcal{H}}^{\lambda} &= \hat{V}^{\lambda} + \hat{T} + \lambda\,\hat{V}_{ee}\\ &= -\frac{\Delta v^{\lambda}\,\Delta\hat{n}}{2} + \hat{T} + \frac{\lambda\,U}{4}\,\left(\hat{N}^2 + \Delta\hat{n}^2\right)\\ &\quad -\frac{\lambda\,U\,\hat{N}}{2}.\end{aligned} \qquad \text{(B.5)}$$

By integrating the Hellmann-Feynman equation between $\lambda = 0$ and $\lambda = 1$ we obtain the following expression for the ground-state energy

$$\begin{aligned}E_0 &= -\frac{\Delta n\,\Delta v}{2} + T_s\\ &\quad +\frac{U}{4}\int_0^1 d\lambda\,\langle\Psi_0^{\lambda}|\hat{N}^2 + \Delta\hat{n}^2|\Psi_0^{\lambda}\rangle - \frac{U\,N}{2}.\end{aligned} \qquad \text{(B.6)}$$

By comparing this expression for E_0 with the definition of the total energy, we extract

$$E_{xc} = \frac{U}{4}\int_0^1 d\lambda\,\langle\Psi_0^{\lambda}|\hat{N}^2 + \Delta\hat{n}^2|\Psi_0^{\lambda}\rangle - U_H - \frac{U\,N}{2}. \qquad \text{(B.7)}$$

The first term in the integrand in equation (B.6) is just N^2, while from equation (10) we find

$$\sum_{m\neq 0}|\langle\Psi_0^{\lambda}|\Delta\hat{n}|\Psi_m^{\lambda}\rangle|^2 = -\frac{1}{\pi}\int_0^{\infty} d\omega\,\mathrm{Im}\,\chi^{\lambda}(\omega). \qquad \text{(B.8)}$$

Inserting this into equation (B.7) we finally have,

$$E_{xc} = -\frac{U}{4\,\pi}\int_0^1 d\lambda\int_0^{\infty} d\omega\,\mathrm{Im}\,\chi^{\lambda}(\omega) - \frac{U\,N}{2}, \qquad \text{(B.9)}$$

where we have made use of the expression of the Hartree energy,

$$U_H = \frac{U}{4}\left(N^2 + \Delta n^2\right). \tag{B.10}$$

We also see that

$$E_x = -\frac{U}{4\,\pi}\int_0^\infty d\omega\,\mathrm{Im}\,\chi^{\lambda=0}(\omega) - \frac{U\,N}{2}, \tag{B.11}$$

where we have made use of the expression of the exchange energy for integer occupations $N = 1,\,2$,

$$E_x = -\frac{U}{4\,N}\left(N^2 + \Delta n^2\right). \tag{B.12}$$

This finally yields,

$$E_c = -\frac{U}{4\,\pi}\int_0^1 d\lambda \int_0^\infty d\omega\,\mathrm{Im}\,\left(\chi^{\lambda}(\omega) - \chi^{\lambda=0}(\omega)\right). \tag{B.13}$$

Equation (B.9) is used to define equation (26) of the main text.

B.3 Generalization to U_i

It is easy to show that any result obtained for the Hubbard dimer can be easily translated to a dimer with different Coulomb energies U_1 and U_2 by simply re-writing the on-site potential and Coulomb terms. For example for $N = 2$, $S^z = 0$ we can use the relationships

$$\Delta v = \Delta v' + \frac{U_2 - U_1}{2}, \quad U = \frac{U_2 + U_1}{2}, \tag{B.14}$$

to write

$$\hat{H} = \begin{pmatrix} 0 & -\sqrt{2}\,t & -\sqrt{2}\,t \\ -\sqrt{2}\,t & -\Delta v' + U_1 & 0 \\ -\sqrt{2}\,t & 0 & \Delta v' + U_2 \end{pmatrix}. \tag{B.15}$$

Similar transformations can be defined for $N = 1, 3$. A corollary is that the solution of the Anderson dimer can be obtained from the solution of its equivalent asymmetric Hubbard dimer. Equation (B.14) can be inserted in equation (8) of the main text.

B.4 Fractional particle number

By inverting the relation

$$\begin{aligned}\Delta n[\Delta v_s, \mathcal{N}] = (1-w)\,\Delta n[\Delta v_s, N] \\ +w\,\Delta n[\Delta v_s, N+1],\end{aligned} \tag{B.16}$$

where $\mathcal{N} = N + w$, and defining $\tilde{\mathcal{N}} = \mathcal{N}$ for $\mathcal{N} \le 2$, $\tilde{\mathcal{N}} = 4 - \mathcal{N}$ for $\mathcal{N} \ge 2$, we find

$$\begin{aligned}\frac{\Delta v_s[\Delta n, \mathcal{N}]}{2\,t} &= \frac{\Delta n}{\sqrt{\tilde{\mathcal{N}}^2 - \Delta n^2}}, \\ r_s[\Delta n, \mathcal{N}] &= \frac{\tilde{\mathcal{N}}}{\sqrt{\tilde{\mathcal{N}}^2 - \Delta n^2}}, \\ c_s^{\pm} &= \frac{1}{\sqrt{2}}\left(1 \mp \frac{\Delta n}{\tilde{\mathcal{N}}}\right)^{1/2}.\end{aligned} \tag{B.17}$$

The above expressions yield

$$\chi_s(\nu) = \frac{4\sqrt{\tilde{\mathcal{N}}^2 - \Delta n^2}}{\tilde{\mathcal{N}}\left(\nu^2 - \frac{\tilde{\mathcal{N}}^2}{\tilde{\mathcal{N}}^2 - \Delta n^2}\right)}, \tag{B.18}$$

that indicates that we can generalize the response function to arbitrary fractional $\mathcal{N}$. Equation (B.18) is used to define the exact expressions of the coefficients in equation (19) of the main text.

Appendix C: Expansions and limits

C.1 Symmetric limit

The energies can be written in terms of $r_u = \sqrt{4 + u^2}$ as

$$e_{0,2} = \frac{1}{2}\left(u \mp r_u\right), \;\; e_1 = u. \quad \text{(sym)} \tag{C.1}$$

The linear response frequencies and weights are

$$\begin{aligned}\nu_1 = \frac{1}{2}\left(u + r_u\right), \quad \nu_2 = r_u, \quad \text{(sym)} \\ W_1 = 2\left(1 - \frac{u}{r_u}\right), \;\; W_2 = 0.\end{aligned} \tag{C.2}$$

The weight of the second excitation is identically zero. The linear response parameters described in the main text are

$$a = \frac{r_u}{8}, \quad b = 0, \quad c = \frac{r_u}{8}\frac{r_u + u}{r_u - u}, \quad \nu_f = r_u. \quad \text{(sym)} \tag{C.3}$$

Finally, the overlap between the exact and KS ground state wavefunctions is

$$\langle \Psi_0 | \Phi_0 \rangle = \frac{2 - u + r_u}{\sqrt{2\,\left[(u - r_u)^2 + 4\right]}}. \quad \text{(sym)} \tag{C.4}$$

Equation (C.2) is used in the discussions after equation (11) and Figure 2.

C.2 Ground-state density functional

The $\mathcal{F}$-functional of the Hubbard dimer looks like

$$\begin{aligned}\mathcal{F}(\rho,u) &= \frac{F(\rho,u)}{2\,t} = \min_{\Psi}\langle\Psi\,|\,\frac{\hat{T}}{2t}+\frac{\hat{V}_{ee}}{2t}\,|\,\Psi\rangle \\ &= \min_{g}\left(-g+h(g,\rho,u)\right),\\ h(g,\rho,u) &= u\,\frac{g^2\left(1-\sqrt{1-g^2-\rho^2}\right)+2\,\rho^2}{2\,(g^2+\rho^2)}.\end{aligned} \tag{C.5}$$

Solving for g in $\partial h/\partial g = 1$ yields a tenth-order equation, that after some tuning can be reduced to the following sixth-order equation

$$p_2(g)\,u^2+p_1(g)\,u+p_0(g)=0, \tag{C.6}$$

where

$$\begin{aligned}p_0 &= (g^2+\rho^2)^2\,(g^2+\rho^2-1),\\ p_1 &= 2\,\rho^2\,g\,(g^2+\rho^2-1),\\ p_2 &= g^2\,((g^2/2+\rho^2)^2-\rho^2).\end{aligned} \tag{C.7}$$

The resulting g_0, when introduced in equation (C.5) delivers the $\mathcal{F}$-functional. This is substituted in the equation $\partial\mathcal{F}/\partial\rho = -x$ to find $z(\rho) = x/u$.

We bring back now the ansatz developed in reference [61], that provides an excellent approximation for the reduced potential $z(\rho)$. This is

$$\begin{aligned}g_0^{app}(\rho) &= \sqrt{\frac{(1-\rho)\,(1+\rho\,(1+(1+\rho)^3\,a_1\,u))}{1+(1+\rho)^3\,a_2\,u}},\\ a_i &= a_{i1}+a_{i2}\,u,\\ a_{21} &= \frac{\sqrt{(1-\rho)\,\rho/2}}{2},\ a_{11}=(1+\rho^{-1})\,a_{21},\\ a_{12} &= \frac{1-\rho}{2},\ a_{22}=\frac{a_{12}}{2}.\end{aligned} \tag{C.8}$$

We show in Figure 3 in the main text that the potential $z(\rho)$ obtained this way provides a very accurate fit to the exact reduced potential.

C.2.1 Weakly correlated functional expansion

We expand the parameter g using the weak coupling expansion $g=\sum_n a_n\,u^n$, and then apply the constraint $\partial h/\partial g = 1$ to find the a_n coefficients for g_0. We find

$$\begin{aligned}g_0 &= \bar{\rho}\left(1-\frac{\bar{\rho}^2\,u^2}{8}+\frac{\rho^2\,\bar{\rho}^{5/2}\,u^3}{4}\right),\\ \mathcal{F} &= -\bar{\rho}\left(1-\frac{(1+\rho^2)\,u}{2}+\frac{\bar{\rho}^2\,u^2}{8}-\frac{\rho^2\,\bar{\rho}^{5/2}\,u^3}{8}\right),\\ |z^{WC}| &= \frac{\rho}{\bar{\rho}\,u}\left(1+\rho\,u+\frac{5\,\bar{\rho}^2\,u^2}{8}\right.\\ &\quad\left.+\frac{(1-4\,\rho^2)\,\bar{\rho}^{5/2}\,u^3}{4}\right),\end{aligned} \tag{C.9}$$

where $\bar{\rho}=\sqrt{1-\rho^2}$. This procedure delivers an accurate estimate of $z(\rho)$ for $u\le 1-2$. We find that adding higher orders than u spoils the estimate. Equation (C.9) is used in equation (34) of the main text.

C.2.2 Strongly correlated functional expansion

The large-u expansion can be found from equation (C.6). We expand $g=\sum_n b_n\,u^{-n}$ and find

$$\begin{aligned}g_0 &= \tilde{\rho}\left(1+\sqrt{\frac{1-\rho}{2\,\rho}}\,\frac{1}{2\,u}\right.\\ &\quad\left.+\frac{3\,(1-3\,\rho)}{16\,\rho\,u^2}+\frac{1-8\,\rho+11\,\rho^2}{8\,\rho\,\tilde{\rho}\,u^3}\right),\\ \frac{\mathcal{F}}{u} &= \rho\left(1-\frac{\tilde{\rho}}{\rho\,u}-\frac{1-\rho}{4\,\rho\,u^2}-\frac{(1-3\,\rho)\,\tilde{\rho}}{16\,\rho^2\,u^3}\right),\\ |z^{SC}| &= 1-\frac{1-2\,\rho}{\tilde{\rho}\,u}+\frac{1}{4\,u^2}+\frac{1+3\,\rho-6\,\rho^2}{16\,\tilde{\rho}\,\rho\,u^3},\end{aligned} \tag{C.10}$$

with $\tilde{\rho}=\sqrt{2\,\rho\,(1-\rho)}$. This procedure provides an accurate estimate of $z(\rho)$ for sufficiently large u, except near $\rho=0$. We have found that including higher orders in the expansion also spoils how z^{SC} fits z. This Appendix is not used in the main text, but is included for completeness.

C.3 Many-body expansion

The Taylor series expansion in powers of u for fixed x can be found by straightforward perturbation theory. A simpler route however consists of expanding θ in equation (A.2) in powers of u. We find to the order given:

$$\begin{aligned}e_{0,2} &= \mp p_0\left(1\mp\left(\frac{1}{2}+x^2\right)\,\tilde{u}+\frac{1/4+x^2}{2}\,\tilde{u}^2\right),\\ e_1 &= p_0\,\tilde{u}\,\left(1+x^4\,\tilde{u}^2\right),\end{aligned} \tag{C.11}$$

where $p_0=\sqrt{1+x^2}$ and $\tilde{u}=u/p_0^3$. The frequencies are

$$\frac{\nu_j}{p_0} = j\left(1+\frac{1+4\,x^2}{8}\,\tilde{u}^2\right)+\delta_{j1}\,\frac{1-2\,x^2}{2}\,\tilde{u}, \tag{C.12}$$

while the weights are

$$\begin{aligned}W_1 &= \frac{1}{p_0^2}\,\left(2+(4\,x^2-1)\,\tilde{u}+2\,x^2\,(3\,x^2-4)\,\tilde{u}^2\right),\\ W_2 &= \frac{x^2}{p_0^2}\,\tilde{u}^2\,\left(1+\left(2\,x^4-4\,x^2-\frac{1}{4}\right)\,\tilde{u}^2\right),\end{aligned} \tag{C.13}$$

and the oscillator strength is

$$f = x^2\,\tilde{u}^2. \tag{C.14}$$

The KS values are

$$\frac{\nu_s}{p_0} = 1 - x^2\,\tilde{u} + \frac{7\,x^2}{8}\,\tilde{u}^2,$$
$$W_s = \frac{2}{p_0^2}\left(1 + 2\,x^2\,\tilde{u} + x^2\left(3\,x^2 - \frac{7}{4}\right)\tilde{u}^2\right). \quad \text{(C.15)}$$

The kernel parameters are, to the order given,

$$a = \frac{p_0}{4}\left(1 - x^2\,\tilde{u} + \left(x^2 + \frac{1}{8}\right)\tilde{u}^2\right),$$
$$b = \frac{9\,x^2\,p_0^3\,\tilde{u}^2}{16}\left(1 - \frac{2}{3}\,p_0\,\tilde{u}\right),$$
$$\nu_f = 2\,p_0\left(1 + \frac{p_0^2\,\tilde{u}^2}{8}\right). \quad \text{(C.16)}$$

Equation (C.16) is used to define equation (33) of the main text.

C.4 Expansion for fixed interaction-asymmetry ratio

We find that equation (A.2) can be written as the following cubic equation for the variable $\cos\theta$:

$$\cos 3\,\theta = \cos\theta\,\left(4\,\cos^2\theta - 3\right) = \frac{9\,z^2 - 1 - 9/(2\,u^2)}{(z_b + 3/u^2)^{3/2}}, \quad \text{(C.17)}$$

where $z_b = 1 + 3\,z^2$. The zeroth order of the above equation in a $1/u$ expansion looks hardly solvable for $\cos\theta$:

$$\cos\theta\,\left(4\,\cos^2\theta - 3\right) = \frac{9\,z^2 - 1}{z_b^{3/2}} \quad (\mathrm{u} \to \infty). \quad \text{(C.18)}$$

However, we note that the second excited state can be written in this limit as

$$e_2 = u\,(1 + z) = \frac{2}{3}\,u\,(1 + z_b^{1/2}\,\cos\theta) \quad \text{(C.19)}$$

so that we find

$$2\,z_b^{1/2}\,\cos\theta(z) = 1 + 3\,z,$$
$$2\,z_b^{1/2}\,\sin\theta(z) = \pm\sqrt{3}\,(1 - z). \quad \text{(C.20)}$$

It is easy to check that this result for $\cos\theta$ solves the cubic equation (C.18). Choosing the plus or minus signs for the sin function yield $e_0 = 0$ or $u\,(1 - z)$ hence rendering the MH or CT regimes, respectively. We can expand now the full θ function in powers of $1/u^2$, and retrieve easily the results found below using the perturbation theory. These results are used to find equation (33) in Section 4.3 and equation (39) in Section 4.5 and equation (40) in Section 4.6.

C.4.1 Perturbative expansion

The basis states $|\varphi_{a,b,c}\rangle$ defined in equation (A.1) become the eigenstates for $u = \infty$, and are the starting point of the perturbative expansion. The ground state is $|\Psi_0\rangle = |\varphi_a\rangle$ if $z < 1$ and $|\Psi_0\rangle = |\varphi_b\rangle$ if $z > 1$. There is therefore a change of limits at $z = 1$ that demands a different expansion for the MH and CT regimes. The dimensionless perturbed energies to third order in $1/u$ are

$$e_a = -\frac{1}{z_a\,u} + \frac{16\,(z^2+1)}{(z_a\,u)^3},$$
$$e_{b,c} = u\,(1 \mp z) + \frac{1}{2\,(1 \mp z)\,u} - \frac{z \pm 1}{8\,z\,((1 \mp z)\,u)^3}, \quad \text{(C.21)}$$

where $z_a = 1 - z^2$, and the corresponding perturbed states to up to order $1/u^4$ are:

$$\alpha_i = g_{\alpha,i}\sum_k f_{\alpha,i}^{(k)}\,u^{-k},$$
$$\beta_i^{\pm} = g_{\beta,i,\pm}\sum_k f_{\beta,i,\pm}^{(k)}\,u^{-k},$$
$$g_{\alpha,a} = g_{\beta,b,+} = g_{\beta,c,-} = 1,$$
$$g_{\alpha,b}(z) = -\frac{1}{\sqrt{2}\,(1-z)},\ g_{\alpha,c}(z) = g_{\alpha,b}(-z),$$
$$g_{\beta,a,\pm} = \mp\frac{1}{\sqrt{2}\,(z \mp 1)},$$
$$g_{\beta,b,-}(z) = -\frac{1}{4\,z\,(1-z)},\ g_{\beta,c,+}(z) = g_{\beta,b,-}(-z),$$
$$f_{\alpha,a}^{(0)} = f_{\alpha,b}^{(1)} = f_{\beta,a,\pm}^{(1)} = f_{\beta,b,+}^{(0)} = f_{\beta,b,-}^{(2)} = f_{\beta,c,+}^{(2)} = f_{\beta,c,-}^{(0)} = 1,$$
$$f_{\alpha,a}^{(2)} = -\frac{z^2+1}{2\,z_a^2},$$
$$f_{\alpha,a}^{(4)} = \frac{3\,z^4 + 30\,z^2 + 11}{8\,z_a^4},$$
$$f_{\alpha,b}^{(3)}(z) = -\frac{2\,z+1}{4\,z\,(1-z)^2},\ f_{\alpha,c}^{(3)}(z) = f_{\alpha,c}^{(3)}(-z),$$
$$f_{\beta,a,\pm}^{(3)} = -\frac{z^2 \pm 2\,z + 3}{2\,z_a^2},$$
$$f_{\beta,b,+}^{(2)}(z) = -\frac{1}{4\,(1-z)^2},\ f_{\beta,c,-}^{(2)}(z) = f_{\beta,b,+}^{(2)}(-z),$$
$$f_{\beta,b,+}^{(4)}(z) = \frac{6\,z^2 + 6\,z - 1}{32\,z^2\,(1-z)^4},\ f_{\beta,c,-}^{(4)}(z) = f_{\beta,b,+}^{(4)}(-z),$$
$$f_{\beta,b,-}^{(4)}(z) = -\frac{3}{4\,(1-z)^2},\ f_{\beta,c,+}^{(4)}(z) = f_{\beta,b,-}^{(4)}(-z). \quad \text{(C.22)}$$

C.4.2 Mott-Hubbard regime $U > \Delta v$

The ordering of states in the MH regime is $0 = a$, $1 = b$, $2 = c$. Then, the excitation energies are:

$$\frac{\nu_{1,2}^{\mathrm{MH4}}}{u} = 1 \mp z \pm \frac{z \pm 3}{2\, z_a\, u^2} \mp \frac{(1 \pm z)^4 \pm 8\, z\, (z^2+1)}{8\, z\, z_a^3\, u^4}, \quad \text{(C.23)}$$

while the weights and oscillator strength are

$$\begin{aligned} W_{1,2}^{\mathrm{MH4}} &= \frac{2}{(1 \mp z)^2\, u^2} - \frac{2\, z^3 \pm 7\, z^2 + 8\, z \mp 1}{z\, (1-z)^4\, (z+1)^2\, u^4} \\ &\quad \pm \frac{2\, (z^5 \pm 8\, z^4 + 23\, z^3 \pm 20\, z^2 + 14\, z \mp 2)}{z\, (1-z)^6\, (z+1)^4\, u^6}, \\ f^{\mathrm{MH4}} &= \frac{1-z}{2} + \frac{3\, z^2 - 1}{4\, z\, z_a\, u^2} - \frac{3\, z^4 - 22\, z^2 + 3}{16\, z\, z_a^3\, u^4}. \end{aligned} \quad \text{(C.24)}$$

The density $\rho = (\beta_0^+)^2 - (\beta_0^-)^2$ is given to second order in t by

$$\rho = \frac{2\, z}{(z_a\, u)^2} \left(1 - \frac{2\, z\, (2 + z^2)}{(z_a\, u)^4}\right). \quad \text{(C.25)}$$

This formula fits very well the exact ρ, although a slight improvement can be gained by using

$$\rho = \frac{2\, z}{z^2 + u^2\, z_a^2}. \quad \text{(C.26)}$$

The kernel parameters are

$$\begin{aligned} a^{\mathrm{MH6}} &= \frac{z_a\, u}{8} \left(1 + \sum_{p=1}^{3} \frac{f_a^{(p)}(z)}{(z_a\, u)^{2\,p}}\right), \\ b^{\mathrm{MH6}} &= \frac{z_a^2\, z^2\, u^3}{2\, z_b} \left(1 + \sum_{p=1}^{3} \frac{f_b^{(p)}(z)}{(z_a^2\, z_b\, u^2)^p}\right), \\ \nu_f^{\mathrm{MH6}} &= z_b^{1/2}\, u \left(1 + \sum_{p=1}^{3} \frac{f_\nu^{(p)}(z)}{(z_a\, z_b\, u^2)^p}\right) \\ f_a^{(1)} &= 2\, (1 + z^2), \\ f_a^{(2,3)} &= -2 - 7\, z^2 + z^4,\ 2\, (1 + 6\, z^2 + z^4), \\ f_b^{(1)} &= 7\, z^4 + 18\, z^2 - 1, \\ f_b^{(2)} &= \frac{37\, z^8 - 152\, z^6 + 202\, z^4 - 352\, z^2 + 9}{4}, \\ f_b^{(3)} &= -\frac{13 + 1063\, z^4 + 219\, z^8 + 49\, z^{12}}{2} \\ &\quad + 383\, z^2 + 1242\, z^6 + 71\, z^{10}, \\ f_\nu^{(1)} &= 2 - z^2, \\ f_\nu^{(2)} &= -\frac{4 - 3\, z^2 + 19\, z^4 - 4\, z^6}{2}, \\ f_\nu^{(3)} &= \frac{8 - 4\, z^2 + 137\, z^4 + 70\, z^6 + 49\, z^8 - 4\, z^{10}}{2}, \end{aligned} \quad \text{(C.27)}$$

where $z_a = (1 - z^2)$, $z_b = 3\, z^2 + 1$. Equation (C.27) is used in equation (39) of the main text. Equations (C.24) and (C.27) are used to plot Figure 9 of the main text.

C.4.3 Charge transfer regime $U < \Delta v$

The ordering of states in the CT regime is $0 = b$, $1 = a$, $2 = c$. Then, the excitation energies, weights and strengths are:

$$\begin{aligned} \nu_1 &= u\, (z-1) + \frac{z+3}{2\, \bar{z}_a\, u} \\ &\quad - \frac{z^4 + 12\, z^3 + 6\, z^2 + 12\, z + 1}{8\, z\, \bar{z}_a^3\, u^3}, \\ \nu_2 &= 2\, z\, u + \frac{z}{\bar{z}_a\, u} - \frac{z^4 + 6\, z^2 + 1}{4\, z\, \bar{z}_a^3\, u^3}, \\ W_1 &= \frac{1}{(z-1)^2\, u^2} \left(2 - \frac{2\, z^3 + 7\, z^2 + 8\, z - 1}{z\, \bar{z}_a^2\, u^2} \right. \\ &\quad \left. + \frac{2\, (z^5 + 8\, z^4 + 23\, z^3 + 20\, z^2 + 14\, z - 2)}{z\, \bar{z}_a^4\, u^4}\right), \\ W_2 &= \frac{1}{z^2\, \bar{z}_a^2\, u^4} \left(1 - \frac{2\, (2\, z^2 + 1)}{\bar{z}_a^2\, u^2} \right. \\ &\quad \left. + \frac{40\, z^6 + 95\, z^4 + 26\, z^2 - 1}{4\, z^2\, \bar{z}_a^4\, u^4}\right), \\ f &= \frac{1}{z\, \bar{z}_a\, (z+1)\, u^2} - \frac{6\, z^3 - 3\, z^2 + 2\, z - 1}{2\, z^2\, \bar{z}_a^3\, (z+1)\, u^4}. \end{aligned} \quad \text{(C.28)}$$

Here $\bar{z}_a = z^2 - 1$. The density is given to second order in t by

$$\Delta n = 2 - \frac{1}{(z-1)^2\, u^2} + \frac{3\, z^2 + 4\, z - 1}{4\, z^2\, (z-1)^4\, u^4}, \quad \text{(C.29)}$$

although the following expression fits the exact Δn better:

$$\Delta n = \frac{4\, u^2\, (1-z)^2}{2\, u^2\, (1-z)^2 + 1}. \quad \text{(C.30)}$$

The kernel parameters are

$$\begin{aligned} a &= \frac{(z-1)}{4}\, u + \frac{z+1}{8\, z\, (z-1)\, u} - \frac{z^2 + 5\, z - 2}{32\, z^2\, (z-1)^3\, u^3}, \\ b &= \frac{(3\, z - 1)^2}{16\, z^3}\, u, \\ &\quad - \frac{(3\, z - 1)\, (18\, z^4 - 46\, z^3 + 31\, z^2 - 8\, z + 1)}{64\, z^6\, (z-1)^2\, u}, \\ \nu_f &= 2\, u\, z + \frac{4\, z^2 - 4\, z + 1}{4\, z^2\, (z-1)\, u} \\ &\quad - \frac{(2\, z - 1)\, (8\, z^4 - 20\, z^3 + 26\, z^2 - 7\, z + 1)}{64\, z^5\, (z-1)^3\, u^3}. \end{aligned} \quad \text{(C.31)}$$

Equations (C.28) and (C.31) are used to plot Figures 9 and 10 of the main text.

C.5 Dissociative limit

We analyse here the states and charge response in the dissociative limit, e.g., $t \to 0$. Within the notation followed in this article, this means $z, u \to \infty$. We find that the many-body and KS ground states match in the dissociative CT regime, but are very different in the dissociative MH regime. We start with the Kohn-Sham response.

C.5.1 Kohn-Sham response

The KS potential in the MH regime is zero, $x_s = 0$. Therefore, $r_s = 1$ and the wave-function coefficients $c_{s,\pm} = 1/\sqrt{2}$. Hence the KS HOMO/LUMO wavefunctions are bonding/antibonding orbitals

$$|\phi^{\pm}\rangle = \frac{|1\rangle \mp |2\rangle}{\sqrt{2}}, \quad \text{(MH)} \tag{C.32}$$

with energies $\mp t$. As a consequence, the three singlet two-particle states are

$$\begin{aligned} |\Phi_0\rangle &= \frac{|12\rangle + |21\rangle + |11\rangle + |22\rangle}{2}, \\ |\Phi_1\rangle &= \frac{|11\rangle - |22\rangle}{\sqrt{2}}, \\ |\Phi_2\rangle &= \frac{|12\rangle + |21\rangle - (|11\rangle + |22\rangle)}{2}. \quad \text{(MH)} \end{aligned} \tag{C.33}$$

We also find that the excitation frequencies and weights are $\nu_s = 1$ and $\nu_d = 2$, $W_s = 2$, $W_d = 0$. Finally, the KS charge response coefficients are $a_s = c_s = 1/4$.

In contrast, the KS potential in the CT regime is $x_s = x - u > 0$. Therefore $r_s = x - u$, the KS HOMO/LUMO are

$$|\phi^{-}\rangle = |1\rangle, \quad |\phi^{+}\rangle = |2\rangle, \quad \text{(CT)} \tag{C.34}$$

with energies $\mp(x-u)/2$. the singlet two-particle KS eigenstates in the dissociative CT regime are

$$\begin{aligned} |\Phi_0\rangle &= |11\rangle, \\ |\Phi_1\rangle &= \frac{1}{\sqrt{2}}\left(|12\rangle + |21\rangle\right), \\ |\Phi_2\rangle &= |22\rangle. \quad \text{(CT)} \end{aligned} \tag{C.35}$$

The excitation frequencies are $\nu_s = x - u$, $\nu_d = 2\,\nu_s$, and the weights are $W_s = 2/(x-u)$ and $W_d = 0$. The coefficients of the response function are $a_s = (x-u)/4$ and $c_s = (x-u)^3/4$. The results of this section are also used in the discussion in Section 5.1.

C.5.2 Many-body response

The eigenstates in the symmetric limit are

$$|\Psi_0\rangle = \frac{|12\rangle + |21\rangle}{\sqrt{2}}, \quad |\Psi_{1,2}\rangle = \frac{|11\rangle \mp |22\rangle}{\sqrt{2}}, \tag{C.36}$$

while in the MH regime are

$$|\Psi_0\rangle = \frac{|12\rangle + |21\rangle}{\sqrt{2}}, \quad |\Psi_1\rangle = |11\rangle, \quad |\Psi_2\rangle = |22\rangle. \tag{C.37}$$

The overlap between the exact and KS ground state wavefunctions in the MH regime is

$$\langle \Psi_0 | \Phi_0 \rangle = \frac{1}{\sqrt{2}}. \quad \text{(MH)} \tag{C.38}$$

The states $|\Psi_0\rangle$ and $|\Psi_1\rangle$ swap their nature at around $z = 1$, so in the CT regime the states are

$$|\Psi_0\rangle = |11\rangle, \quad |\Psi_1\rangle = \frac{|12\rangle + |21\rangle}{\sqrt{2}}, \quad |\Psi_2\rangle = |22\rangle. \tag{C.39}$$

The overlap between the exact and KS ground state wavefunctions in the MH regime is 1. We analyze only the MH regime from now on because the CT formulas are rather cumbersome and are not used in our interpolation. We find that the excitation frequencies and weights are

$$\nu_{1,2} = u \mp x, \quad W_i = \frac{2}{\nu_i^2}. \quad \text{(MH)} \tag{C.40}$$

Then, the kernel parameters are

$$\begin{aligned} a &= \frac{1}{2\,\nu_3} = \frac{u^2 - x^2}{8\,u}, \quad b = \frac{(u^2 - x^2)^2}{2\,u\,(u^2 + 3\,x^2)}, \\ c &= \frac{\nu_1\,\nu_2}{2\,\nu_4} = \frac{(u^2 - x^2)^3}{8\,u\,(u^2 + 3x^2)}, \\ \nu_f^2 &= \frac{\nu_1\,\nu_2\,\nu_3}{\nu_4} = u^2 + 3\,x^2. \quad \text{(MH)} \end{aligned} \tag{C.41}$$

Equation (C.36) is used in equation (43) of the main text. The results of this section are also used in the discussion in Sections 3 and 5.1.

References

1. E. Runge, E.K.U. Gross, Phys. Rev. Lett. **52**, 997 (1984)
2. C.A. Ullrich, *Time-dependent density-functional theory: concepts and applications* (Oxford University Press, Oxford, 2011)
3. M.A. Marques, N.T. Maitra, F.M. Nogueira, E.K. Gross, A. Rubio, Eds., in *Fundamentals of time-dependent density functional theory* (Springer-Verlag, Berlin, Heidelberg, 2012), Vol. 837
4. M. Casida, *Recent advances in density functional methods, Part I* (World Scientific, Singapore, 1995)
5. M.E. Casida, in *Recent developments and applications of modern density functional theory* (Elsevier, Amsterdam, 1996), p. 391
6. R.A.R. Bauernschmitt, Chem. Phys. Lett. **256**, 454 (1996)
7. T. Grabo, M. Petersilka, E. Gross, J. Mol. Struct. (Theochem) **501**, 353 (2000)
8. K. Yabana, T. Nakatsukasa, J.-I. Iwata, G. Bertsch, Phys. Status Solidi B **243**, 1121 (2006)
9. N.T. Maitra, J. Chem. Phys. **144**, 220901 (2016)

10. C. Adamo, D. Jacquemin, Chem. Soc. Rev. **42**, 845 (2013)
11. D. Jacquemin, V. Wathelet, E.A. Perpète, C. Adamo, J. Chem. Theory Comput. **5**, 2420 (2009)
12. P. Elliott, F. Furche, K. Burke, in *Excited states from time-dependent density functional theory* (Wiley, Hoboken, NJ, 2009), pp. 91–165
13. M. Casida, M. Huix-Rotllant, Annu. Rev. Phys. Chem. **63**, 287 (2012)
14. M.E. Casida, M. Huix-Rotllant, in *Density-Functional Methods for Excited States*, edited by N. Ferré, M. Filatov, M. Huix-Rotllant (Springer International Publishing, Cham, 2016), pp. 1–60
15. D. Tozer, R. Amos, N. Handy, B. Roos, L. Serrano-Andres, Mol. Phys. **97**, 859 (1999)
16. A. Dreuw, J.L. Weisman, M. Head-Gordon, J. Chem. Phys. **119**, 2943 (2003)
17. D. Tozer, J. Chem. Phys. **119**, 12697 (2003)
18. O. Gritsenko, E.J. Baerends, J. Chem. Phys. **121**, 655 (2004)
19. N.T. Maitra, J. Chem. Phys. **122**, 234104 (2005)
20. N.T. Maitra, J. Phys.: Condens. Matter **29**, 423001 (2017)
21. Y. Tawada, T. Tsuneda, S. Yanagisawa, T. Yanai, K. Hirao, J. Chem. Phys. **120**, 8425 (2004)
22. T. Stein, L. Kronik, R. Baer, J. Am. Chem. Soc. **131**, 2818 (2009)
23. R. Baer, E. Livshits, U. Salzner, Ann. Rev. Phys. Chem. **61**, 85 (2010)
24. L. Kronik, T. Stein, S. Refaely-Abramson, R. Baer, J. Chem. Theory Comput. **8**, 1515 (2012)
25. T. Körzdörfer, J.-L. Brédas, Acc. Chem. Res. **47**, 3284 (2014)
26. D.S.C. Jamorski, M.E. Casida, J. Chem. Phys. **104**, 5134 (1996)
27. D. Tozer, N. Handy, Phys. Chem. Chem. Phys. **2**, 2117 (2000)
28. N.T. Maitra, F. Zhang, R.J. Cave, K. Burke, J. Chem. Phys. **120**, 5932 (2004)
29. S. Tretiak, V. Chernyak, J. Chem. Phys. **119**, 8809 (2003)
30. P. Elliott, S. Goldson, C. Canahui, N.T. Maitra, Chem. Phys. **391**, 110 (2011)
31. R.J. Cave, F. Zhang, N.T. Maitra, K. Burke, Chem. Phys. Lett. **389**, 39 (2004)
32. G. Mazur, M. Makowski, R. Wldarczyk, Y. Aoki, Int. J. Quantum Chem. **111**, 819 (2011)
33. G. Mazur, R. Wlodarczyk, J. Comput. Chem. **30**, 811 (2009)
34. M. Huix-Rotllant, A. Ipatov, A. Rubio, M.E. Casida, Chem. Phys. **391**, 120 (2011)
35. J.P. Bergfield, Z.-F. Liu, K. Burke, C.A. Stafford, Phys. Rev. Lett. **108**, 066801 (2012)
36. G. Stefanucci, S. Kurth, Phys. Rev. Lett. **107**, 216401 (2011)
37. E. Dagotto, Rev. Mod. Phys. **66**, 763 (1994)
38. P.A. Lee, N. Nagaosa, X.-G. Wen, Rev. Mod. Phys. **78**, 17 (2006)
39. P.W. Anderson, J. Phys. Conf. Ser. **449**, 012001 (2013)
40. R. Baer, J. Chem. Phys. **128**, 044103 (2008)
41. Y. Li, C.A. Ullrich, J. Chem. Phys. **129**, 044105 (2008)
42. C. Verdozzi, Phys. Rev. Lett. **101**, 166401 (2008)
43. S. Kurth, G. Stefanucci, E. Khosravi, C. Verdozzi, E.K.U. Gross, Phys. Rev. Lett. **104**, 236801 (2010)
44. I.V. Tokatly, Phys. Rev. B **83**, 035127 (2011)
45. J.I. Fuks, M. Farzanehpour, I.V. Tokatly, H. Appel, S. Kurth, A. Rubio, Phys. Rev. A **88**, 062512 (2013)
46. M. Farzanehpour, I.V. Tokatly, Phys. Rev. B **86**, 125130 (2012)
47. R. Requist, O. Pankratov, Phys. Rev. A **81**, 042519 (2010)
48. P. Schmitteckert, M. Dzierzawa, P. Schwab, Phys. Chem. Chem. Phys. **15**, 5477 (2013)
49. J.I. Fuks, N.T. Maitra, Phys. Chem. Chem. Phys. **16**, 14504 (2014)
50. J.I. Fuks, N.T. Maitra, Phys. Rev. A **89**, 062502 (2014)
51. N. Dittmann, J. Splettstoesser, N. Helbig, Phys. Rev. Lett. **120**, 157701 (2018)
52. S. Kurth, G. Stefanucci, arXiv:1803.03244 (2018)
53. A. Kartsev, D. Karlsson, A. Privitera, C. Verdozzi, Sci. Rep. **3**, 2570 (2013)
54. D. Karlsson, C. Verdozzi, M.M. Odashima, K. Capelle, EPL **93**, 23003 (2011)
55. L. Mancini, J.D. Ramsden, M.J.P. Hodgson, R.W. Godby, Phys. Rev. B **89**, 195114 (2014)
56. V. Turkowski, T.S. Rahman, J. Phys.: Condens. Matter **26**, 022201 (2014)
57. R. Requist, O. Pankratov, Phys. Rev. B **77**, 235121 (2008)
58. D.J. Carrascal, J. Ferrer, Phys. Rev. B **85**, 045110 (2012)
59. K. Capelle, V.L. Campo Jr., Phys. Rep. **528**, 91 (2013)
60. F. Aryasetiawan, O. Gunnarsson, Phys. Rev. B **66**, 165119 (2002)
61. D.J. Carrascal, J. Ferrer, J.C. Smith, K. Burke, J. Phys.: Condens. Matter **27**, 393001 (2015)
62. M. Thiele, S. Kümmel, Phys. Rev. Lett. **112**, 083001 (2014)
63. M. Ruggenthaler, S.E.B. Nielsen, R. van Leeuwen, Phys. Rev. A **88**, 022512 (2013)
64. P. Hohenberg, W. Kohn, Phys. Rev. **136**, B864 (1964)
65. E. Gross, W. Kohn, Phys. Rev. Lett. **55**, 2850 (1985)
66. M.A. Marques, N.T. Maitra, F.M. Nogueira, E.K. Gross, A. Rubio (Eds.), in *Fundamentals of time-dependent density functional theory* (Springer-Verlag, Berlin, Heidelberg, 2012), Vol. 837, Chap. 1
67. W. Thomas, Naturwissenschaften **13**, 627 (1925)
68. W. Kuhn, Z. Phys. **33**, 408 (1925)
69. F. Reiche, W. Thomas, Z. Phys. **34**, 510 (1925)
70. G. Mahan, *Many-particle physics*, 3rd edn. (Springer, New York, 2000)
71. P.F. Maldague, Phys. Rev. B **16**, 2437 (1977)
72. D. Baeriswyl, C. Gros, T.M. Rice, Phys. Rev. B **35**, 8391 (1987)
73. W. Kohn, Phys. Rev. **133**, A171 (1964)
74. D. Langreth, J. Perdew, Solid State Commun. **17**, 1425 (1975)
75. O. Gunnarsson, B. Lundqvist, Phys. Rev. B **13**, 4274 (1976)
76. C. Li, R. Requist, E.K.U. Gross, J. Chem. Phys. **148**, 084110 (2018)
77. A.G.O.V. Gritsenko, S.J.A. van Gisbergen, E. Baerends, J. Chem. Phys. **113**, 8478 (2000)